UNCLASSIFIED

AD 278 118

Reproduced
by the

ARMED SERVICES TECHNICAL INFORMATION AGENCY
ARLINGTON HALL STATION
ARLINGTON 12, VIRGINIA

UNCLASSIFIED

NOTICE: When government or other drawings, specifications or other data are used for any purpose other than in connection with a definitely related government procurement operation, the U. S. Government thereby incurs no responsibility, nor any obligation whatsoever; and the fact that the Government may have formulated, furnished, or in any way supplied the said drawings, specifications, or other data is not to be regarded by implication or otherwise as in any manner licensing the holder or any other person or corporation, or conveying any rights or permission to manufacture, use or sell any patented invention that may in any way be related thereto.

NOTICE: When government or other drawings, specifications or other data are used for any purpose other than in connection with a definitely related government procurement operation, the U. S. Government thereby incurs no responsibility, nor any obligation whatsoever; and the fact that the Government may have formulated, furnished, or in any way supplied the said drawings, specifications, or other data is not to be regarded by implication or otherwise as in any manner licensing the holder or any other person or corporation, or conveying any rights or permission to manufacture, use or sell any patented invention that may in any way be related thereto.

278 1118

CATALOGED BY ASTIA
AS AD No. 278118

R 192

Technical Report

STATIC AND DYNAMIC LOADING OF PRETENSIONED CONCRETE BEAMS

15 June 1962

U. S. NAVAL CIVIL ENGINEERING LABORATORY

Port Hueneme, California

NOX

ASTIA
JUL 20 1962
TISIA A

STATIC AND DYNAMIC LOADING OF PRETENSIONED CONCRETE BEAMS

Y-F008-10-102A

Type C Final Report

by

S. K. Takahashi

OBJECT OF TASK

To determine how flexural members should be designed, how to gain the greatest resistance to blast loading, where they should be used, and the best way to destroy structures composed of such members.

ABSTRACT

Nine simply supported pretensioned beams were tested in the blast simulator either statically or dynamically. In the dynamic tests the beams were subjected to long- and short-duration loading. As expected, the load capacity of the beams subjected to short-duration loads was greater than that of those subjected to long-duration loads. The deflection-time traces showed that no tensile stresses occurred in the top fiber for any of the loads applied and that a permanent deformation can be considered negligible for loads less than 85 percent of the ultimate load.

A method of predicting the static ultimate deflection is presented and applied to one of the beams. The experimental data is compared with the theory. All of the statically tested beams failed in bond near the supports. In the dynamic tests, two beams failed by concrete compression at mid-span, and the rest failed in bond. A solution for dynamic response, which includes damping, is shown and applied to one of the tests.

Qualified requesters may obtain copies of this report from ASTIA.
This research supported by the Defense Atomic Support Agency.

CONTENTS

page

APPENDICES

INTRODUCTION

In this test series, nine beams were tested to obtain information on the resistance-time relation, recoverability, bond- and shear-resistance, and other response characteristics of pretensioned beams. The tests were conducted at the U. S. Naval Civil Engineering Laboratory, Port Hueneme, California, and were sponsored by the Defense Atomic Support Agency.

The use of prestressed concrete to resist blast loads has received little consideration in the past because of the small negative moment resistance of such members. Upward loading might occur when the members rebounded after being subjected to positive or downward loads of short duration. This report is concerned with the validity of this concept.

The investigation is justified by advantages which could be achieved through the use of prestressed concrete in blast-resistant structures; viz., (1) prestressed beams retain little or no permanent deflection even for loads very near their ultimate; (2) savings in steel, concrete, and floor-to-ceiling clearance can be achieved by using prestressed beams in place of reinforced concrete beams. These characteristics offer marked advantages when the properties of prestressed members can be utilized.

Many static tests have been conducted on pretensioned concrete beams,[1,2] but information is lacking on the behavior of pretensioned beams under blast loading. A series of dynamic tests on post-tensioned concrete beams[3] has shown that sizeable negative (upward) deflections occurred under short-duration loading in beams with a prestressed distribution of 2,000 psi on the bottom and 0 psi on the top. The beams exhibited a high capacity for recovery; thus, essentially all of the energy-absorbing ability of the members was utilized without incurring serious permanent damage.

The approach used in the investigation of the pretensioned members reported here was to explore the general characteristics of behavior. The limited number of members did not permit a detailed investigation of the influence of any one parameter. In the paragraphs which follow, the experimental work is described, the test results and theory are discussed, and the implications of the results are set down. An application of static theory for determining the load-deflection relation of a pretensioned beam throughout the entire range of loading is given in Appendix A. An example of dynamic analysis is shown in Appendix B.

EXPERIMENTAL WORK

Description and Construction of Test Members

Nine simply supported pretensioned concrete beams, 8 inches wide by 12 inches deep by 13 feet long, were tested, some statically and some dynamically. The clear span length was 12 feet 4 inches.

The beams contained fourteen, 1/4-inch-diameter, plain prestressing wires, two in the top and twelve in the bottom. Two No. 4 deformed reinforcing bars were also included in the upper portion of the beam. The properties of the prestressing steel and the deformed reinforcing steel are given in Table 1. The stress-strain curve for the prestressing steel is given in Figure 1.

Table 1. Mechanical Properties of Prestress Steel and Reinforcing Steel

Prestressing Steel (1/4-inch-dia.)	Stress (psi)
Proportional limit, f_p	152,000
Yield strength (0.2% offset), f_{yp}	217,800
Tensile strength, f_u	242,200
Elastic modulus of elasticity, E_{ss}	28.8×10^6
Plastic modulus, E'_{ss}	2.55×10^6
Rate of loading = 30,000 psi per minute	

Reinforcing Steel (1/2-inch-dia.)	Stress (psi)
Yield strength, f_y	50,000
Tensile strength, f_u	78,100
Elastic modulus of elasticity, E_s	28.4×10^6
Plastic modulus, E'_s	0
Rate of loading = 30,000 psi per minute	

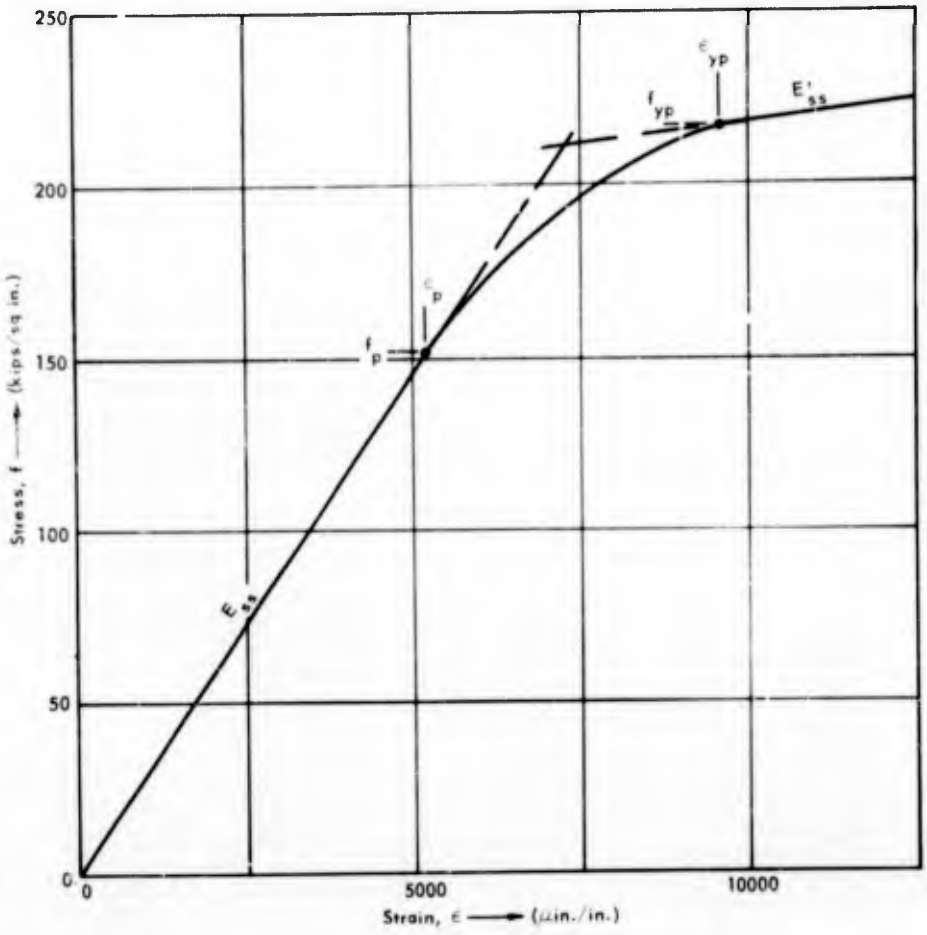

Figure 1. Average stress-strain curve for prestressing steel.

Three days prior to casting the beams, the high-tensile-strength wires were stressed with hydraulic jacks on a prestressing bed as shown in Figures 2 and 3. Three forms were placed in series with the steel wires passing through them so that only one prestressing operation was necessary for each three beams. The initial prestressing force, before releasing the jacks, varied from 99,400 to 100,200 pounds for the three separate castings. The load was determined with two 100,000-pound-capacity load cells wired to a Type M strain indicator (Figure 4) and was measured at each stage of the prestressing and casting operations.

The concrete for casting the beams was mixed in a 16-cubic-foot rotating drum mixer. The mixing time varied between two and four minutes. Internal and external vibration was used after placing the concrete in the forms. After seven days, the forms were removed.

Six standard test cylinders were cast for each beam. Three of the test cylinders from each beam were fog-cured, and they were tested after seven days. The other three cylinders were cured in the field with the beams and were tested with the beams. Three hours after casting, the exposed surfaces of the beams and test cylinders were painted with a clear curing compound.

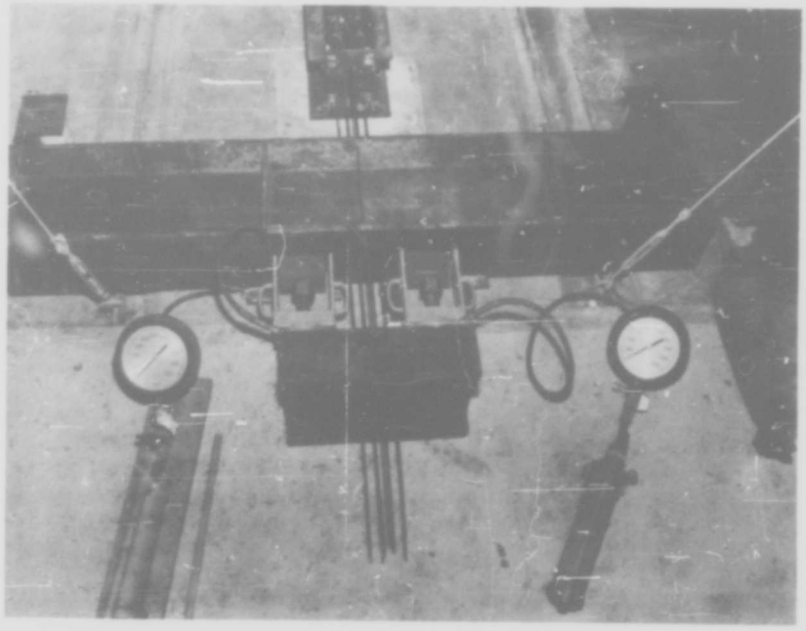

Figure 2. Close-up of jacking device.

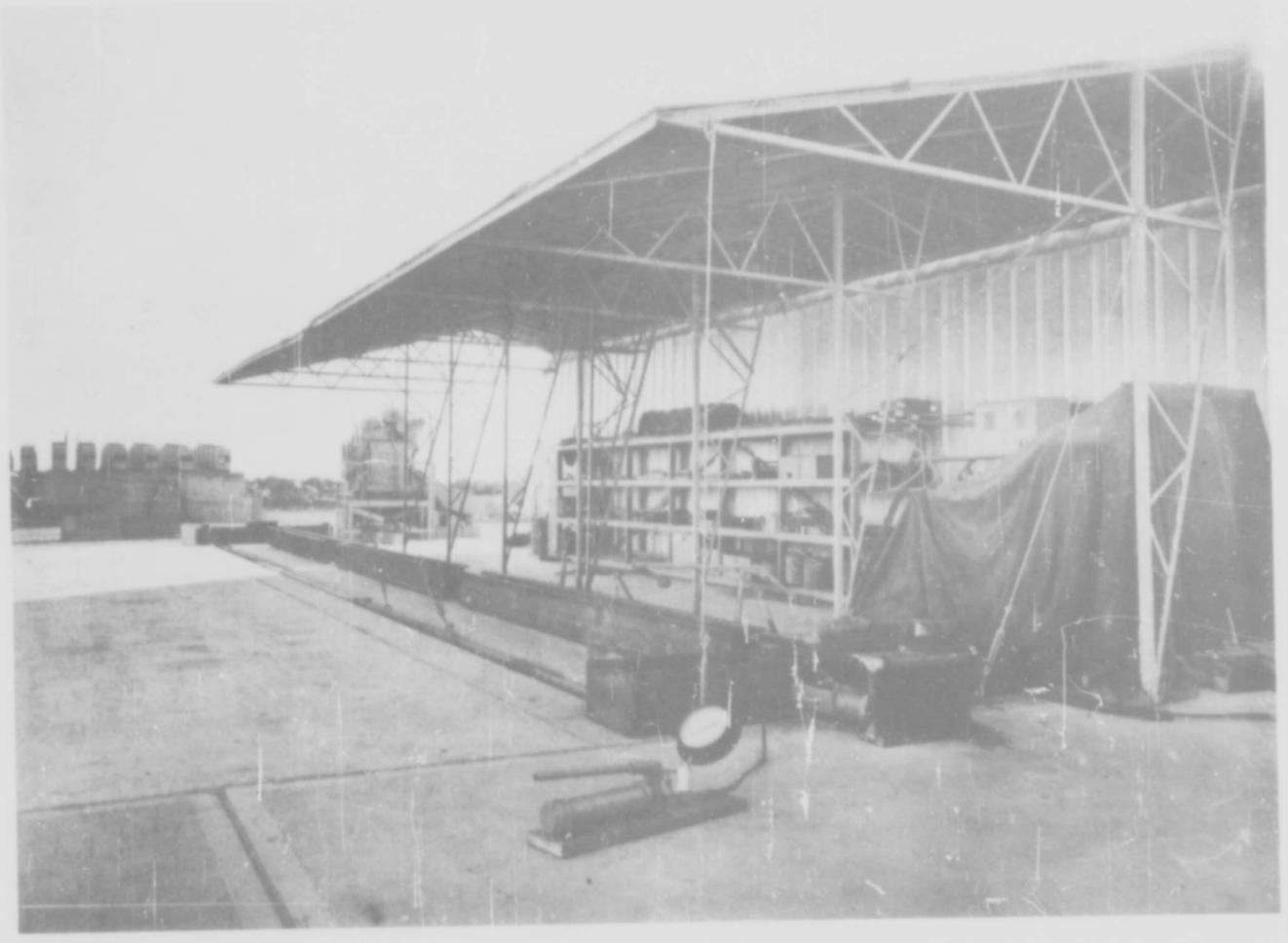

Figure 3. Overall view of prestressing set-up.

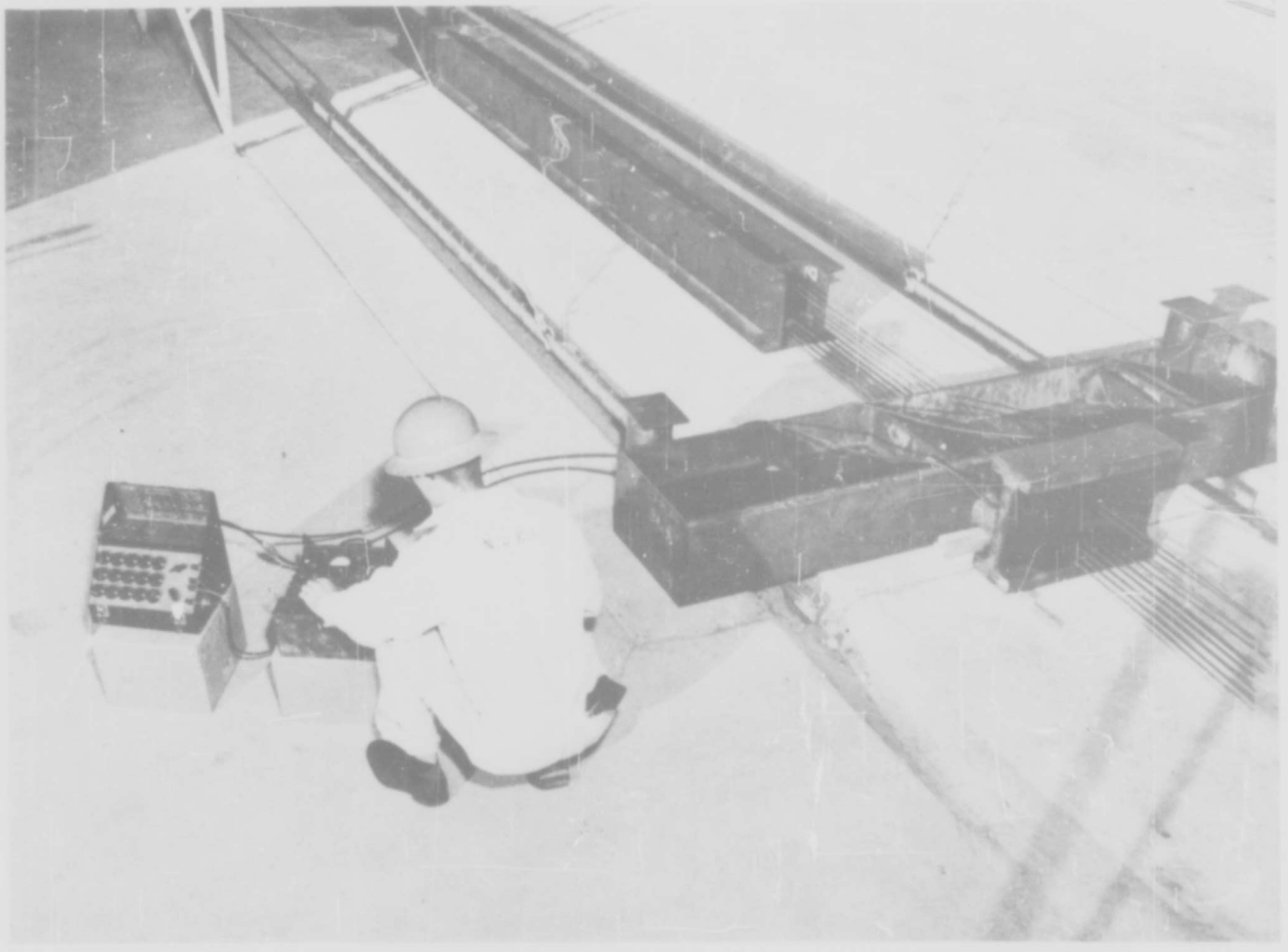

Figure 4. Set-up for measuring load during prestressing operation.

A sieve analysis of the gravel and sand used is given in Table II. High-early-strength concrete was used which provided concrete with a compressive strength of approximately 5,000 psi in seven days. When the beams were tested, the ultimate compressive strength of the concrete varied from 6,410 to 8,370 psi (Table III).

Table II. Sieve Analysis of Gravel and Sand

Percent retained on each sieve, cumulative (average of two trials)

	Sieve	Percent
Gravel	3/8-inch	0.2
	No. 4	75.0
	No. 8	95.0
	No. 16	97.9
	No. 30	100.0
	No. 50	100.0
	No. 100	100.0
	Fineness modulus =	568.1 ÷ 100 = 5.68
Sand	No. 4	1.0
	No. 8	11.0
	No. 16	27.5
	No. 30	52.2
	No. 50	79.6
	No. 100	96.6
	Fineness modulus =	267.9 ÷ 100 = 2.68

Loading Apparatus and Instrumentation

All of the nine pretensioned beams were tested either statically or dynamically in the blast simulator (Figure 5).

The uniformly distributed load consists of gas pressure acting along the top surface of the beam. Leakage is prevented by a neoprene seal (Figure 6). Static loads are applied by pumping air into the simulator from a compressor. Dynamic loads are produced by detonating high explosives within the firing tube in the simulator.[4] A blast loading is produced which has a rise time of approximately 1 millisecond followed by an exponential decay of controlled duration. In past experiments the blast simulator has proved to be very effective in producing this type of loading.[3, 5, 6]

Table III. Average Properties of Concrete*
(6-inch by 12-inch cylinders)

Beam No.	Age (days)	Ult. Compr. Strength (psi)	Static		Dynamic		
			E† (psi)	Poisson's Ratio	Trans. E† (psi)	Long. E† (psi)	Poisson's Ratio
A	8 60	4,780 6,480	3.53	0.149	4.50	4.70	0.248
B	8 64	5,420 7,290	3.71	0.222	4.10	4.33	0.227
C	8 93	4,690 7,070	3.64	0.181	5.07	5.16	0.248
D	7 59	5,200 6,880	3.64	0.148	5.17	5.42	0.218
E	7 55	5,140 6,690	3.46	0.178	4.26	4.59	0.290
F	7 68	5,210 6,410	3.66	0.180	5.47	5.55	0.212
G	7 62	5,760 8,370	4.06	0.190	5.77	5.98	0.222
H	7 48	5,950 8,300	3.90	0.136	4.43	4.53	0.213
K	7 68	5,220 8,040	3.80	0.176	4.43	4.55	0.237

* Tests made in accordance with:

1. ASTM Designation C39-49, Test for compressive strength of molded concrete cylinders
2. ASTM Designation C215-60, Test for fundamental transverse, longitudinal, and torsional frequencies of concrete specimens

† E is in millions (10^{-6}).

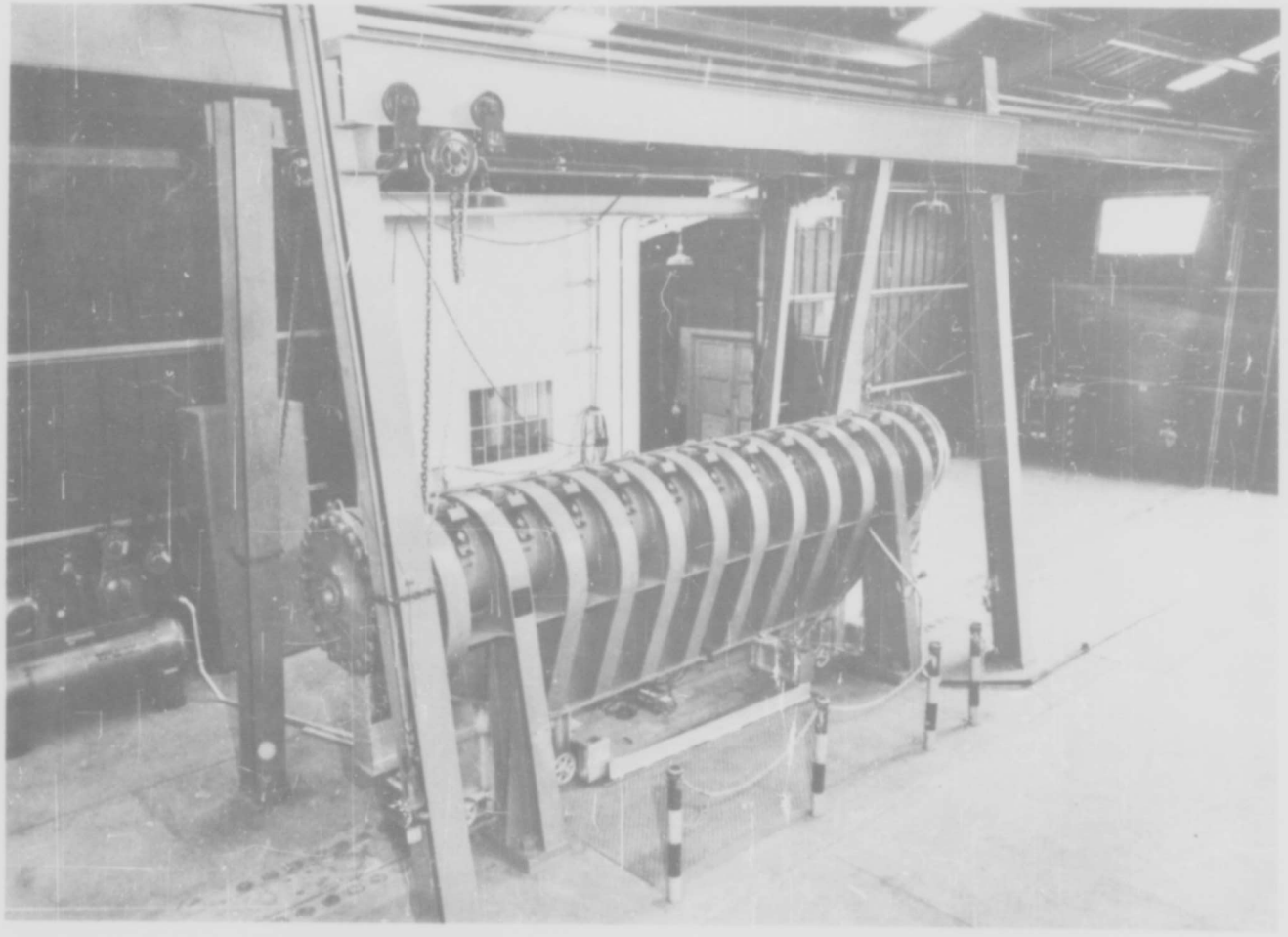

Figure 5. View of the blast simulator.

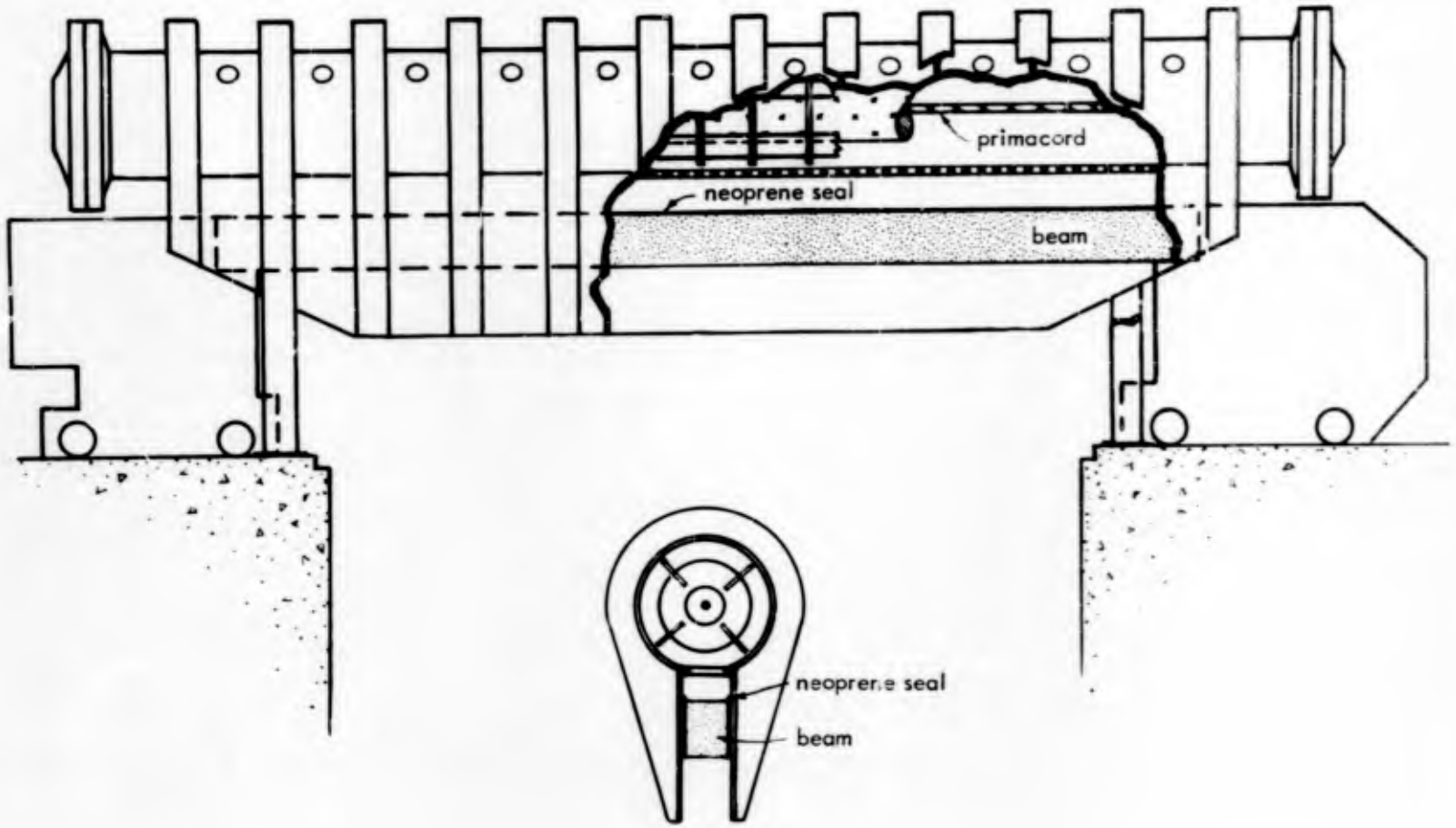

Figure 6. Pictorial and sectional view of the blast simulator.

Instrumentation of the test specimens consisted of strain gages, pressure cells, deflection gages, and an accelerometer located as shown in Figure 7. Strain gages 1, 2, and 3 were mounted on the prestressing wires, and 4 and 5 were mounted on the compression mild steel. The traces from these transducers were recorded by an oscillograph through suitable amplifiers. Deflection-time traces were obtained from two independent measuring devices: 6-inch linear potentiometer and a rotating-drum deflection gage. The latter gage is a revolving drum on which graph paper is mounted to record the deflection. As the beam deflects, a pencil attached to the mid-span of the beam inscribes a deflection-time trace on the graph paper. The drum revolves at a constant rate so that 1 inch is equivalent to 100 milliseconds.

THEORY

The basic principles of pretensioned concrete beams may be briefly stated as:

1. Tensioning the prestressing wires to the desired value before casting the concrete;

2. Transferring the load from the wires to the concrete, which applies an allowable compressive stress below the neutral axis of the beam; and

3. Loading the beam with the design or working load which decreases the compression in the lower fiber without introducing tensile stresses.

Stresses involved in a pretensioned concrete beam may be generalized into three basic groups:

1. Stresses due to initial prestressing force and to dead load;

2. Stresses due to the changing properties of concrete, such as elastic shortening, creep and shrinkage; and

3. Stresses due to live loads on the beam.

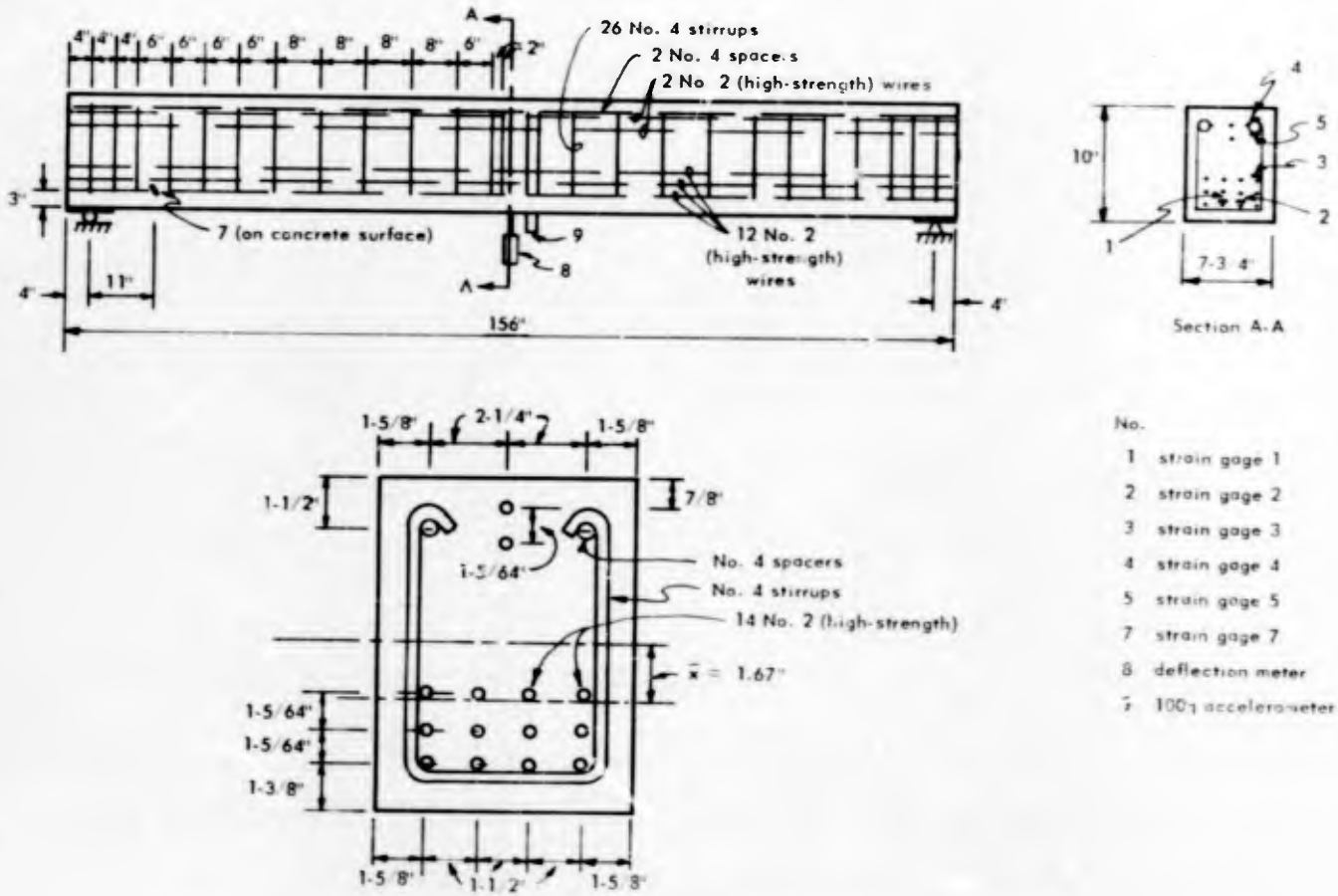

Figure 7. Pretensioned concrete beam dimensions inclucing instrumentation locations.

Static Load-Deflection Curve

To simplify the calculation of the static load-deflection curve, the usual concrete design[7] assumptions were made:

1. A plane section before bending remains plane for all loadings.

2. Concrete tensile strength is negligible.

3. The stress-strain relationship for concrete in compression is given by the idealized curve.

4. Ultimate load and deflection are reached when the outer fibers of concrete in compression reach an ultimate strain.

5. The concrete and mild steel strains are constant throughout the portion of the beam in which yield has occurred.

With these assumptions, the concrete stresses after the prestressed loads are transferred to the beam were taken as: (a) compressive stresses in the top fiber, $f_{ci}^{T} = 0$, and (b) compressive stresses in the bottom fiber, $f_{ci}^{B} = 2,000$ psi. (Nomenclature is listed at the end of this report.) When the beam is loaded on the top surface, compressive stresses are introduced above the neutral axis and compressive stresses are reduced below the neutral axis. Figures 8A and 8B are diagrams for the pre-loading and the loaded stages (shown in two parts). The stress-strain diagrams for the prestress steel below the neutral axis are shown in Figure 9. Point u in diagrams B and C represents the level of stress just prior to testing time; point v indicates the stress value in a loaded condition. The derivations of the stress value f_v at point v follow:

Prestress Steel (tension side)

a. Elastic range (Figure 9B)

When the beam is loaded statically, the compressive strain in the extreme concrete fiber increases by ϵ_c. The strain in the tensile steel is then obtained from diagram A as $[\epsilon_c(d - c)]/a$. By multiplying this strain by E_{ss}, the incremental stress increase is obtained. This value is added to the prestress value prior to testing time, f_{ssi}, which yields point v. Thus the total strain in the steel is $f_v = f_{ssi} + [\epsilon_c(d - a)E_{ss}]/a$.

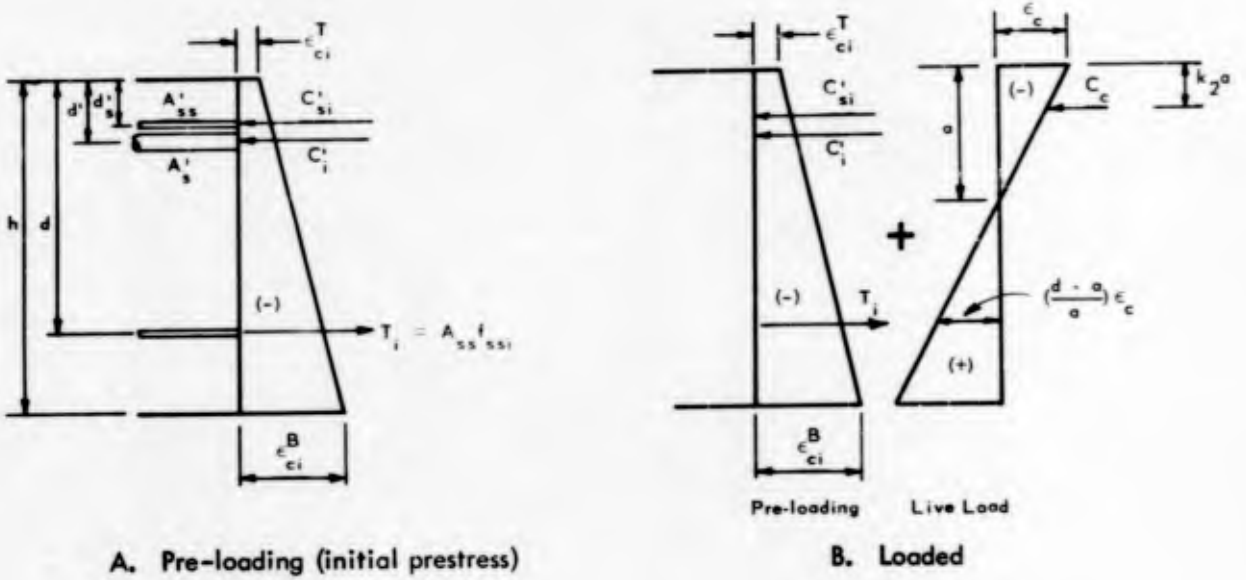

Figure 8. Internal loads and strains of beam cross section at mid-span.

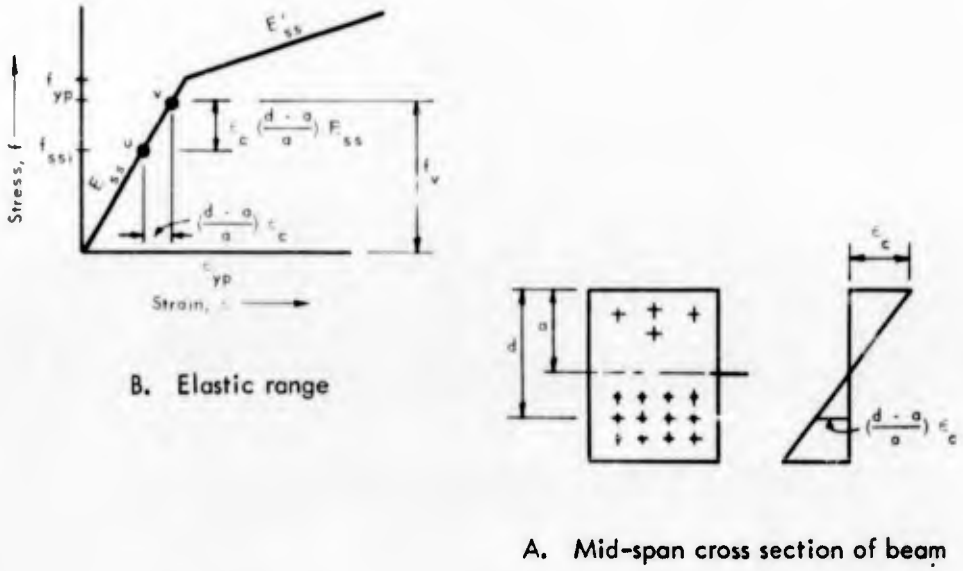

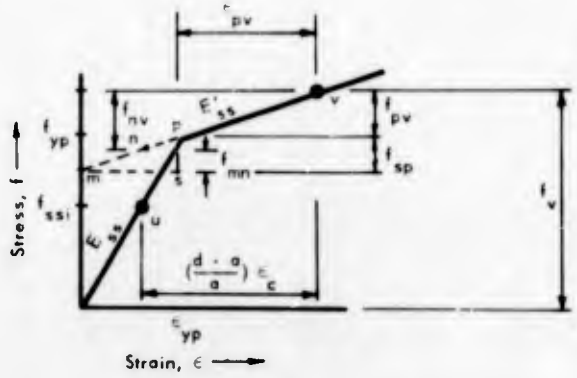

C. Plastic range

Figure 9. Stress-strain diagrams for prestress steel (tension side).

b. Plastic range (Figure 9C)

When the beam is loaded into the plastic range, the modulus of elasticity reduces to E'_{ss} as indicated. The increase in steel strain is again obtained from diagram A as $[\epsilon_c(d - a)]/a$. From diagram C, the stress increment $f_{mn} = (f_{ssi}/E_{ss}) \times E'_{ss}$. The stress from $\underline{n}$ to $\underline{v}$ is $f_{nv} = [\epsilon_c(d - a)E'_{ss}]/a$. Subtracting $f_{sp} = \epsilon_{yp}E'_{ss}$ from $f_{mv} = f_{mn} + f_{nv}$, we have

$$f_{pv} = (\epsilon_{mv} - \epsilon_{yp})E'_{ss} = \left[\frac{f_{ssi}}{E_{ss}} + \frac{\epsilon_c(d - a)}{a} - \epsilon_{yp}\right]E'_{ss}$$

Adding f_{pv} to the yield-point stress gives

$$f_v = f_{yp} + \left[\frac{f_{ssi}}{E_{ss}} + \frac{\epsilon_c(d - a)}{a} - \epsilon_{yp}\right]E'_{ss}$$

Prestress Steel (compression side)

By a similar procedure, the stress at any time in the elastic range is

$$f_v = f'_{ssi} - f_{uv} = f'_{ssi} - \frac{\epsilon_c(a - d'_s)E_{ss}}{a}$$

and for the plastic range

$$f_v = -f_{yp} + f_{sv} = -f_{yp} + \left[\frac{-\epsilon_c(a - d'_s)}{a} + \frac{f'_{ssi}}{E_{ss}} + \epsilon_{yp}\right]E'_{ss}$$

Compression Steel

The stress in the steel for loading in the elastic range is

$$f_v = -f'_s - \frac{\epsilon_c (a - d') E_s}{a}$$

In the plastic range the mild steel is assumed to have a constant stress after yielding. Therefore $f_v = -f_y$.

The equations of tensile and compression forces in the steel are obtained by multiplying the stress by the appropriate areas and are summarized below:

Prestress Steel (tension side)

$$T = A_{ss}\left[f_{ssi} + \epsilon_c\left(\frac{d - a}{a}\right)E_{ss}\right] \qquad (T \leq A_{ss} f_{yp}) \qquad (1)$$

$$T = A_{ss}\left\{f_{yp} + \left[\frac{f_{ssi}}{E_{ss}} + \epsilon_c\left(\frac{d - a}{a}\right) - \epsilon_{yp}\right]E'_{ss}\right\} \qquad (T \geq A_{ss} f_{yp}) \qquad (2)$$

Prestress Steel (compression side)

$$C'_s = A'_{ss}\left[f'_{ssi} - \epsilon_c\left(\frac{a - d'_s}{a}\right)E_{ss}\right] \qquad (C'_s \leq A'_{ss} f_{yp}) \qquad (3)$$

$$C'_s = A'_{ss}\left\{-f_{yp} + \left[\frac{f'_{ssi}}{E_{ss}} + \epsilon_{yp} - \epsilon_c\left(\frac{a - d'_s}{a}\right)\right]E'_{ss}\right\} \qquad (C'_s \geq A'_{ss} f_{yp}) \qquad (4)$$

Mild Steel (compression side)

$$C_s = A'_s\left[-\epsilon_c\left(\frac{a - d''}{a}\right)E_s - f'_s\right] \qquad (C_s \le A'_s f_y) \qquad (5)$$

$$C_s = -A'_s f_y \qquad (C_s \ge A'_s f_y) \qquad (6)$$

Concrete (compression side)

$$C_c = -mba \text{ (Reference 7)} \qquad (C_c \le 0.85 f''_c) \qquad (7)$$

$$m = \frac{1}{3\epsilon_c}\left[\epsilon_c(2f''_c + f'_c) - f_c\epsilon_o\right] \qquad (0 \le \epsilon_c \le \epsilon_o) \qquad (8)$$

$$m = \frac{1}{2\epsilon_c}\left[\frac{f''_c(3\epsilon_c + \epsilon_o)}{3} + f_c(\epsilon_c - \epsilon_o)\right] \qquad (\epsilon_o \le \epsilon_c \le \epsilon_u) \qquad (9)$$

$$f''_c = k_3 f'_c$$

$$k_3 = \frac{3,900 + 0.35 f'_c}{3,000 + 0.82 f'_c - \frac{f'^2_c}{26,000}}$$

$$\epsilon_o = \frac{2f''_c}{E_c}$$

$$E_c = 1,800,000 + 460 f'_c$$

$$\epsilon_u = 0.004 - \frac{f'_c}{6.5 \times 10^6}$$

To find the neutral axis at any time, all the forces are added and set equal to zero:

$$T + C_s' + C_s + C = 0 \tag{10}$$

The equation above will be in the form of a quadratic equation in terms of "a."

If any steel has gone beyond the yield point or ϵ_c is greater than ϵ_o, new expressions for the forces and a revised "a" will have to be obtained. An additional check of forces will then be required. The resisting moment at mid-span can then be found by taking moments about the tension side prestress steel:

$$M = C(d - k_2 a) + C_s(d - d') + C_s'(d - d_s') \tag{11}$$

Next, the applied load is found from the equation:

$$w = \frac{8M}{L^2} \tag{12}$$

If the beam has not yielded, the deflection at mid-span can be found by the moment-area, conjugate beam, or other methods. After the beam yields, the unit rotation diagram method is adopted.[7] Figure 10 shows the loaded beam, the moment diagram, and the unit rotation diagram at ultimate load. The width of the plastic hinge is calculated from the formula

$$\alpha L = L\sqrt{1 - \frac{w_o}{w}} \tag{13}$$

and the maximum ordinate of the unit rotation diagram is $(\epsilon_c + \epsilon_s)/d$. From Figure 10, the mid-span deflection of the beam by moment-area is

$$y = \frac{A_2 \bar{x}}{E_c I} + A_1\left(\frac{L}{4}\right)(2 - \alpha) \tag{14}$$

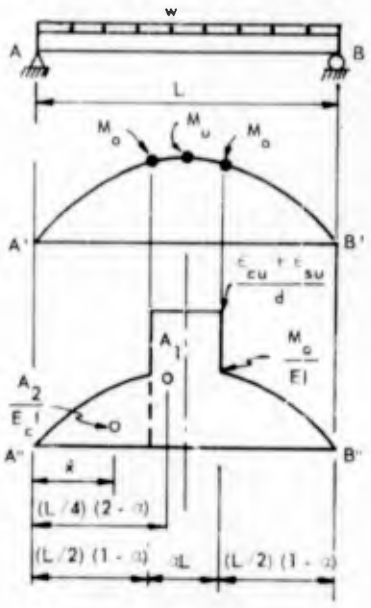

Figure 10. Unit rotation diagram for uniformly loaded beam at ultimate load.

An example for calculating the theoretical static load deflection curve up to the ultimate load is given in Appendix A.

Dynamic Deflection-Time Curve

There are several ways to solve the equation of motion of a simply supported beam subjected to a blast load in the elastic range: Laplace transform, phase-plane, numerical, etc. In this paper, the differential equation of motion of a simply supported beam is first converted to a single-degree-of-freedom system and solved by the Laplace transform method.

Consider a triangular load function imposed on a simply supported beam. If a conversion is made into an idealized single-degree-of-freedom system, then by energy consideration, the mass, m, of the beam is multiplied by a constant 0.78 (Reference 8) and is represented by m_e. The mid-span deflection, the

stiffness of the beam, and the loading function will not be altered by this transformation. Including viscous damping, c, the differential equation of motion of the spring-mass system may be written as

$$m_e \ddot{y} + c\dot{y} + ky = P_o\left(1 - \frac{t}{t_e}\right) \tag{15}$$

where k = stiffness of beam

P_o = peak dynamic load

t = time

t_e = effective load duration

At time-equal-to-zero, the deflection and velocity of the beam at mid-span are zero. Using these initial conditions, the general solution is

$$y = \frac{P_o}{k}\left[1 + \frac{e^{-\zeta\omega t}\left(\frac{1}{\omega t_e} - \zeta - \frac{2\zeta^2}{\omega t_e}\right)\sin\left(\omega\sqrt{1-\zeta^2}\, t\right)}{\sqrt{1-\zeta^2}}\right.$$

$$\left. - e^{-\zeta\omega t}\left(\frac{2\zeta}{\omega t_e} + 1\right)\cos\left(\omega\sqrt{1-\zeta^2}\, t\right) - \frac{t}{t_e} + \frac{2\zeta}{\omega t_e}\right] \tag{16}$$

As an example, the above equation is used to calculate the theoretical deflection-time curve for Beam A, test 2, which was loaded in the elastic range (see Appendix B).

TEST RESULTS AND DISCUSSION

Change in Prestress

Prestress loss in the pretensioned beam occurs from the time the high-strength steel is tensioned after the concrete is poured and to the time the structural member is loaded. Initially a portion of the loss may occur from the elastic movement of the supports that anchor the steel after the jacks are released and from the creep

in steel in the tensioned condition. At a later stage, when the concrete is poured and begins to harden, shrinkage of the concrete further releases the strain in the steel. And finally, when the tendons are cut and the load is transferred, elastic shortening of the concrete takes place, which further releases the stress in the wires. Concrete creep and shrinkage losses continue still further until the beams are tested.

Stresses and strains in the prestressing steel and mild steel from the "initial prestressing" phase to the "before testing" phase are given in Tables IV and V respectively. Table VI gives the accumulated prestress losses. After the load was transferred from the prestressing bed to the beams, the pretensioning was maintained by bond between the concrete and the steel; the ends of the wires were not anchored to the ends of the beams. Total loss in strain of the prestressing steel varied between 20 to 30 percent.

Static Tests

Three simply supported beams (B, H, and K) were tested to failure. In all three cases, bond failure occurred near the ends of the beams as shown in Appendix C, Figures C-2, C-8, and C-9. A sample calculation verifying the mode of failure of Beam B is shown in Appendix D. Of the three beams, Beam H sustained the highest load of approximately 260 lb/linear inch. Bond slippage occurred at an earlier stage for Beams B and K. Figures E-1, E-2, and E-3 (in Appendix E) show the plot of the static resistance-deflection curve. Figures E-4, E-5, and E-6 (also in Appendix E) show the plot of beam resistance against strain for strain gages 1 through 5.

Vibration Tests

The vibration tests were performed by wedging a short wooden column beneath the mid-span of the beam and suddenly knocking the column out with a sledge hammer. The subsequent vibration of the beam was recorded with the oscillograph. The natural period averaged 33 milliseconds.

The damping factor, ζ, is obtained from the equation,[9]

$$\zeta = \frac{\delta}{2\pi} = \frac{\ln\left(\frac{x_n}{x_{n+1}}\right)}{2\pi} \qquad (17)$$

where the logarithmic decrement, δ, is defined as the natural logarithm of the ratio of any successive deflection amplitude of the deflection-time, the strain-time, or other response curve. These deflection amplitudes were obtained from the oscillogram records of the vibration tests.

Table IV. Stress-Strain Values of Prestressing Wires Prior to Beam Loading

d = 0.250 in. f_u = 242,200 psi

f_y = 217,800 psi E = 28.8 × 10^6 psi

ϵ_y = 7,560 μin./in.

1	2	3	4	5	6	7	8	9	10	11	12	13
Beam No.	Initial Prestress		Release Jacks		Before Casting		Prior to Trans.		After Trans.		Before Test	
	Stress (ksi)	Strain (μin./in.)	Stress (ksi)	Strain (μin./in.)	Stress (ksi)	Strain (μin./in.)	Stress (ksi)	Strain (μin./in.)	Stress (ksi)	Strain (μin./in.)	Stress (ksi)	Strain (μin./in.)
A	144.5	5,020	141.2	4,910	138.3	4,910+	134.3	4,770	112.1	4,000	111.0	3,960
B	144.5	5,020	141.2	4,910	138.3	4,910+	133.3	4,740	109.9	3,920	101.6	3,650
C	144.5	5,020	141.2	4,910	138.3	4,910+	132.4	4,700	114.4	4,080	101.6	3,630
D	145.8	5,060	143.8	4,990	142.0	4,990	137.9	4,850	117.0	4,120	104.1	3,670
E	145.8	5,060	143.8	4,990	142.0	4,990	139.6	4,910	120.6	4,250	104.8*	3,700*
F	145.8	5,060	143.8	4,990	142.0	4,990	137.5	4,830	114.8	4,050	101.8*	3,600*
G	144.8	5,020	142.8	4,950	141.8	4,950	137.5	4,800	123.9	4,300	111.5	3,900
H	144.8	5,020	142.8	4,950	141.8	4,950	138.4	4,830	120.8	4,220	103.9	3,630
K	144.8	5,020	142.8	4,950	141.8	4,950	138.6	4,840	121.1	4,230	103.8	3,630

+ Same strain as in Column 5, assuming rigid supports

* Approximate values

Table V. Stress-Strain Values of Mild Steel Prior to Beam Loading

Beam No.	Strain Gage No.	Zero Reading, Strain (μin./in.)	After Load Transfer, Strain (μin./in.)	Difference From Zero, Strain (μin./in.)	Before Test, Strain (μin./in.)	Difference From Zero, Strain (μin./in.)	Average Strain (μin./in.)	Stress in Steel (psi)
A	4	12,330	12,070	260	12,230	100	460*	13,680
	5	10,010	9,760	250	9,920	90		
B	4	11,450	11,310	140	11,530	-80	460*	13,680
	5	10,980	10,790	190	10,990	-10		
C	4	11,730	11,560	170	11,320	410	460	13,470
	5	10,170	9,960	210	9,670	500		
D	4	11,080	10,810	270	10,560	520	580	17,580
	5	10,260	9,950	310	9,610	650		
E	4	10,900	10,630	270	—	—	456*	13,680
	5	11,700	11,420	280	—	—		
F	4	10,480	10,260	220	—	—	456*	13,680
	5	10,540	10,290	250	—	—		
G	4	11,720	11,480	240	11,240	480	380	11,700
	5	10,310	10,080	230	10,020	290		
H	4	11,310	11,120	190	10,900	410	440	13,350
	5	11,420	11,200	220	10,940	480		
K	4	10,500	10,320	180	10,130	370	400	12,240
	5	12,620	12,400	220	12,180	440		

* Use 456 for beams with no value or with erratic strain measurements.

Table VI. Average Accumulated Prestress Losses

Beams	Initial Prestress (ksi)	Release Jacks (ksi)	Before Casting 2.5 days (ksi)	Before Transfer 7 days (ksi)	After Transfer 7 days (ksi)	Before Test 64 days (ksi)
A, B, C	144.5	3.3	6.2	11.2	32.3	39.8
D, E, F	145.8	2.0	3.8	7.5	28.3	42.2
G, H, K	144.8	2.0	3.0	6.6	22.9	38.4

From Beams B and K, the damping factor was 1.61 and 1.34 percent of critical damping, respectively. In comparison, the damping factor of similar post-tensioned beams[3] was 1.59 percent.

Blast Tests

The six remaining beams were tested dynamically under long- and short-duration loads. Long duration is defined here as being any effective load duration that is greater than 8 times the natural period of the beam. The effective duration is obtained by passing a straight line through the peak pressure and the pressure of time t corresponding to the maximum deflection of the member. The experimental natural period was approximately 33 milliseconds per cycle. In the tests, the ratio of effective duration to the natural period of the member was 3 for the short-duration loading and 18 for the long-duration loading. A typical plot of load versus time is shown in Figure 11. The effective load-time curves are shown in dashed lines. The majority of the beams were loaded more than once to determine a wider range of dynamic response. Views of the dynamically tested beams after loading tests are shown in Appendix C.

A summary of the dynamic test data is tabulated in Table VII. Beam G was the only one subjected to short-duration loadings. In these tests, the neoprene seal, usually placed on top of the beam to create an air-tight chamber, was left out so that pressure could leak out at a rapid rate along the sides of the beam. The peak-load and maximum-deflection values from Table VII are plotted in Figure 12, and the static load-deflection curve of Beam H is plotted for comparison. From this figure, the dynamic load factor, which is the ratio of dynamic to static deflection of a member subjected to the same load, in the elastic range for the time ratio $t_e/T_n = 18$, is approximately equal to 2. For the time ratio $t_e/T_n = 3$, the dynamic load factor is slightly greater than 1. Typical oscillogram records are given in Figures 13 and 14.

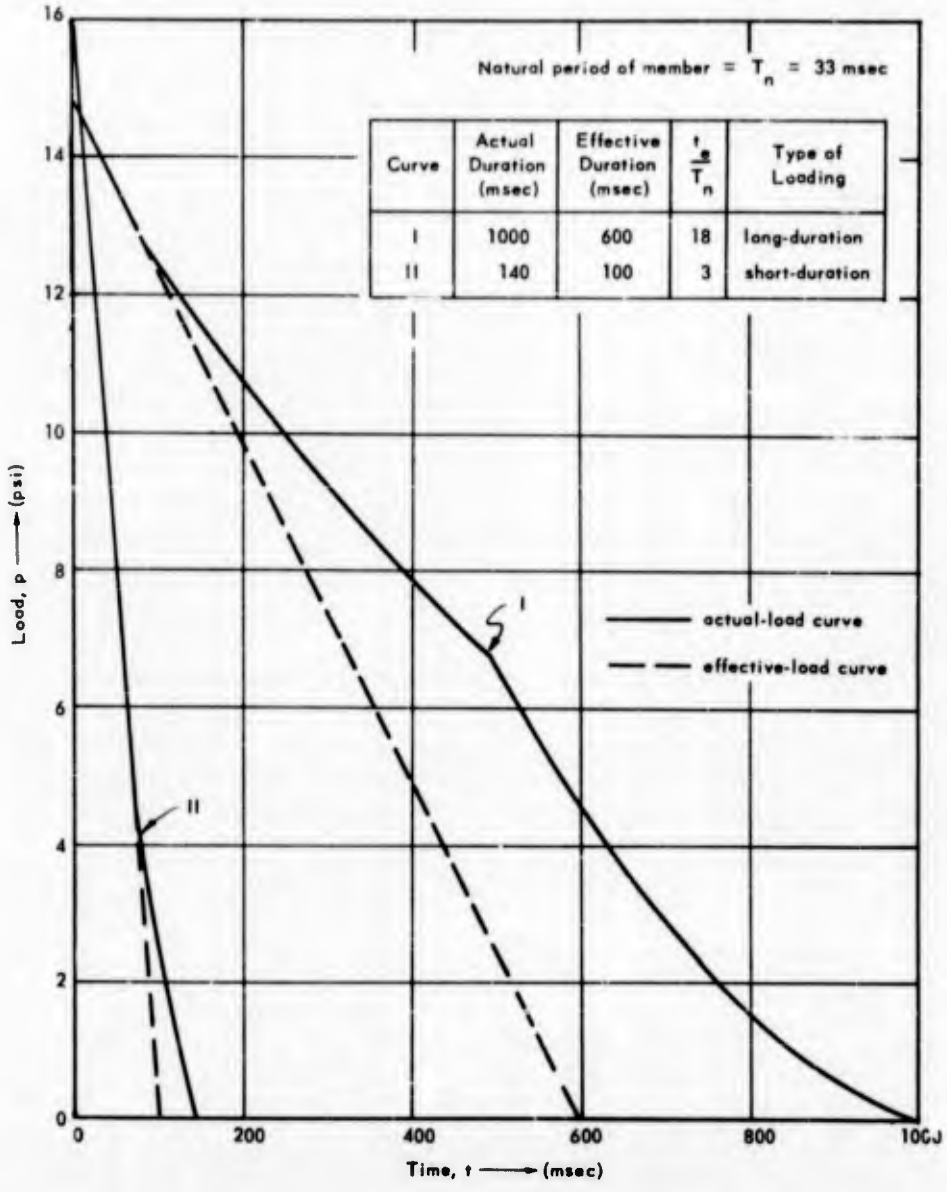

Figure 11. Typical load-time curves for long- and short-duration loads.

Table VII. Summary of Dynamic Test Data

Test No.	Beam No.	Peak Load (lb/in.)	Max. Defl. (in.)	Time to Max. Defl. (msec)	Perm. Defl. (in.)	Maximum Strains (μinch per inch)						Permanent Strains (μinch per inch)						Peak Acc.	
						SG 1	SG 2	SG 3	SG 4	SG 5	SG 7	SG 1	SG 2	SG 3	SG 4	SG 5	SG 7	Pos. (g)	Neg. (g)
1	A	41.1	0.15	—	0	230	220	90	250	220	20	—	—	—	—	—	—	9	10
2	A	65.9	0.30	20	0	580	580	230	—	440	30	—	—	—	—	—	—	15	11
3	A	106.4	0.54	22	0.03	1,340	1,370	750	850	670	40	—	—	—	—	—	—	25	15
4	A	163.9	1.18	27	0.05	2,910	2,900	1,840	1,170	920	40	140	180	40	60	50	10	34	12
5	A	223.6	2.70	42	0.75	4,660	4,320	2,830	—	—	30	1,610	870	640	—	—	30	41	19
6	E	127.4	0.90	24	0.05	2,140	2,070	1,330	780	820	20	20	70	20	100	30	0	29	14
7	E	162.0	1.45	33	0.08	3,290	3,030	2,210	1,190	1,030	10	90	100	90	90	20	0	40	16
8	D	204.9	1.65	32	0.23	3,680	3,950	2,420	1,490	1,150	—	100	110	80	320	200	—	38	15
9	F	223.9	2.87	57	1.60	2,810	2,510	1,680	1,040	750	—	910	320	270	90	30	—	46	22
12*	G	127.8	0.37	13	0	730	740	370	510	430	—	10	10	20	30	80	0	27	16
13*	G	53.8	0.14	12	0	250	210	150	170	50	—	0	0	0	10	30	—	12	13
14*	G	64.8	0.17	14	0	300	250	180	200	60	20	0	0	0	20	40	0	13	17
15*	G	194.4	0.82	23	0.03	2,460	2,120	1,360	820	490	—	190	190	50	60	20	0	31	19
16*	G	223.0	1.52	26	0.06	3,660	4,030	2,800	1,140	690	—	450	390	190	60	60	10	58	29
17*	G	264.4	2.65	39	0.65	5,640	6,460	50	3,110	2,370	—	—	2,110	580	550	940	—	67	26
18	G	75.3	0.36	15	0.02	710	730	380	490	440	90	10	20	10	30	10	—	27	13
19	G	118.8	0.74	25	0.04	1,690	1,830	1,110	740	620	100	70	60	40	90	30	0	27	12
20	C	188.3	1.75	32	0.16	3,690	4,170	2,530	1,120	810	100	80	40	20	240	150	10	26	15
21	C	198.6	2.21	37	0.53	4,020	4,580	3,060	1,080	760	50	40	40	160	110	30	0	48	24

* No neoprene seal was placed on beam. Short duration loading. The rest were subjected to long-duration loads.

Note: Tests 10 and 11 data for beam G was not taken.

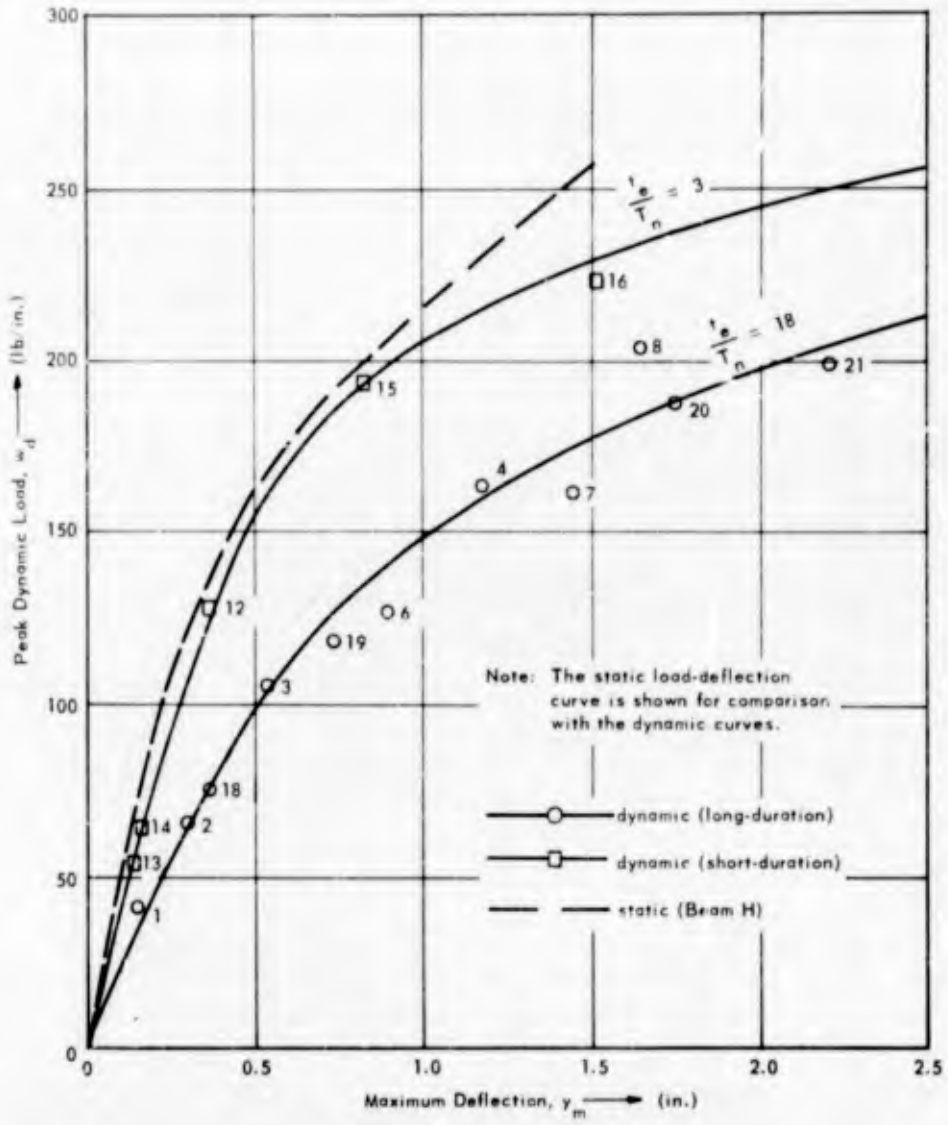

Figure 12. Plot of peak dynamic load versus initial maximum deflection for short- and long-duration loads.

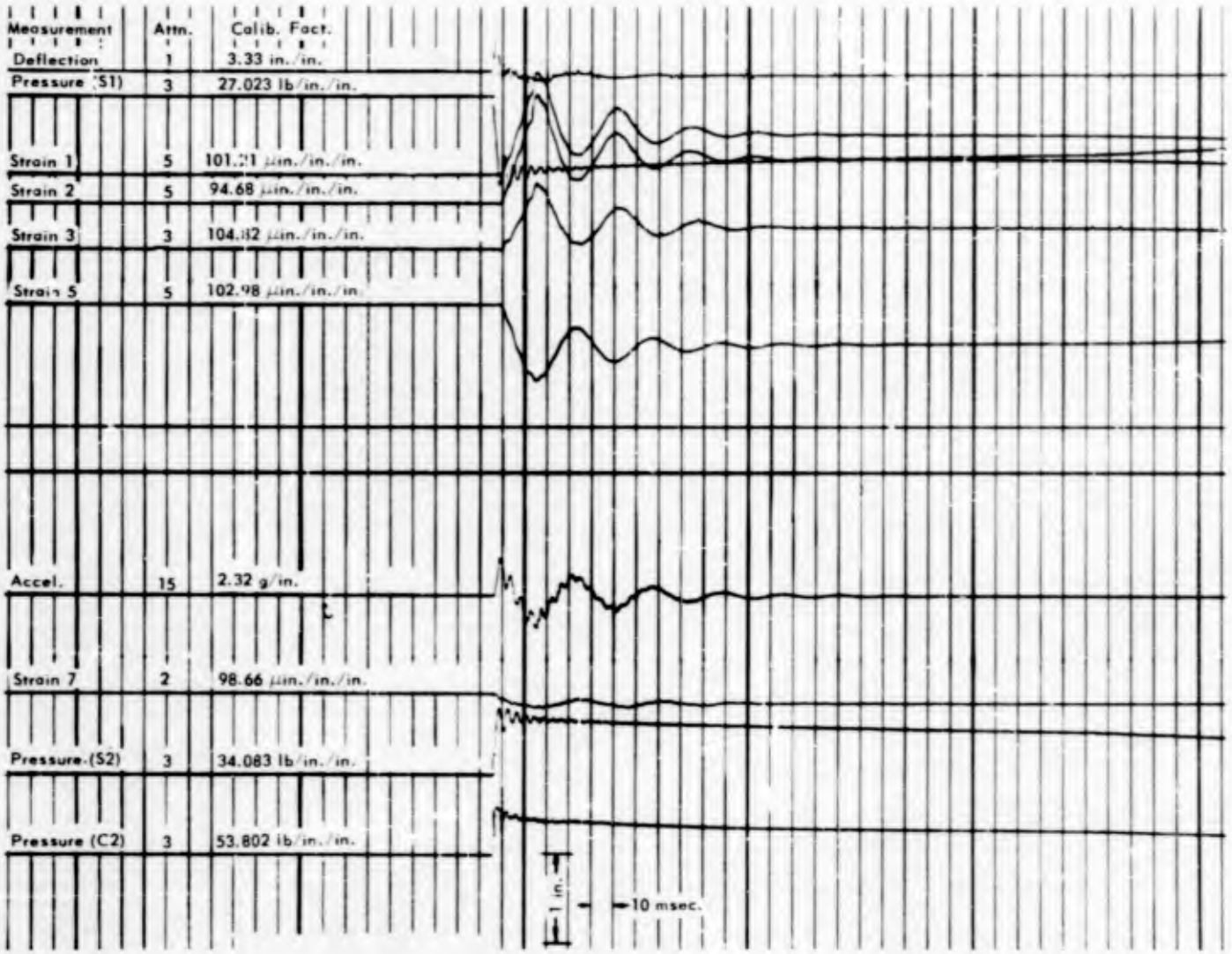

Figure 13. Oscillogram for Beam A, Test 2.

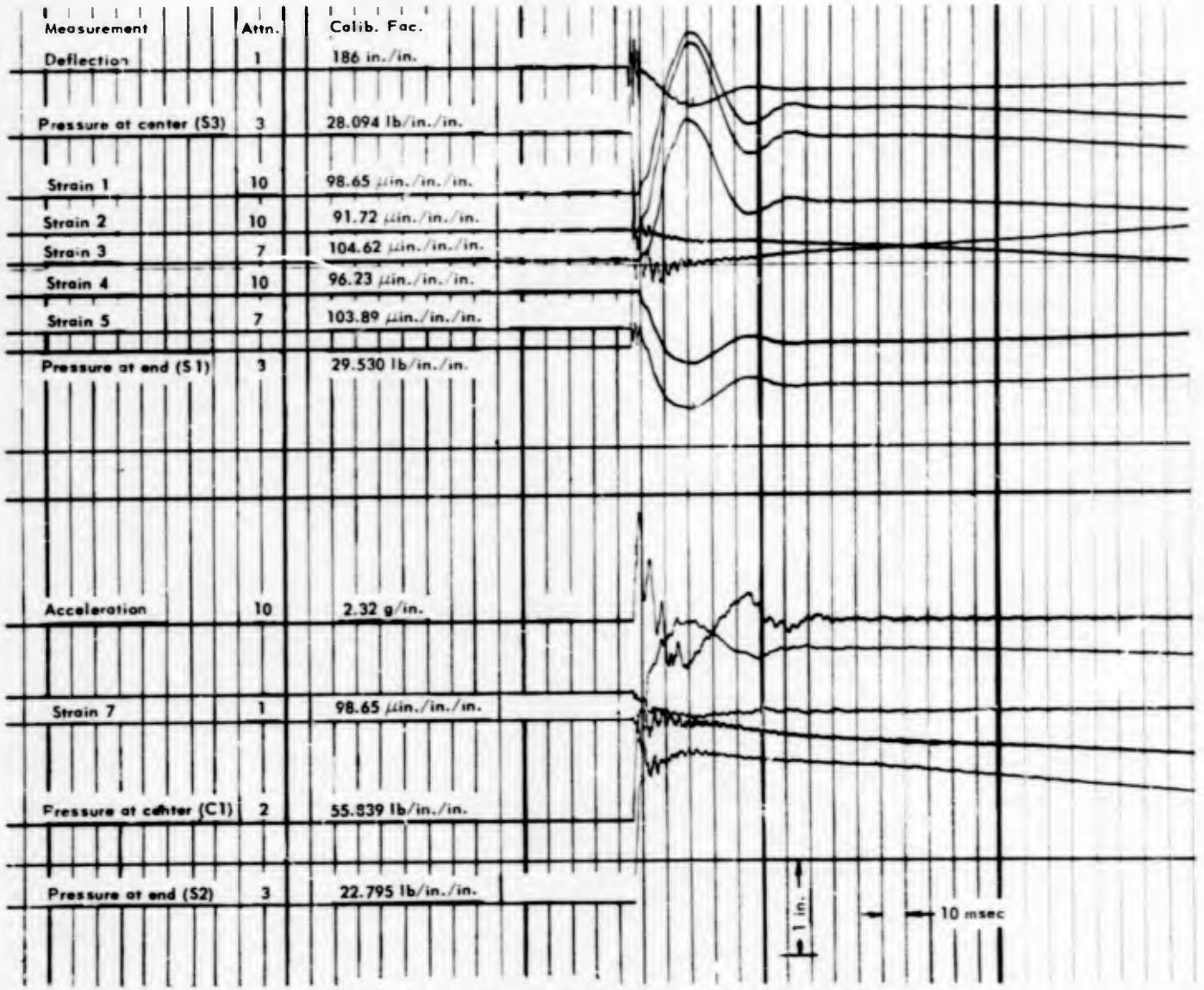

Figure 14. Oscillogram for Beam C, test 19.

The rotating drum traces are shown in Figures F-1 to F-5 in Appendix F; no tensile stress was introduced in the top fiber at any time for any dynamic load. This does not mean that negative deflections would not occur if the load durations were extremely short.

One of the desirable characteristics of a prestressed beam is the ability to recover to nearly its original position if the applied load is not too great. To show the behavior of these prestressed beams, a plot of permanent deflection versus peak load for both long- and short-duration loads is presented in Figure 15. The graph shows that permanent deflections can be assumed negligible to about 85 percent of the failure load.

Bond and Shear

Figures C-1 to C-9 (Appendix C) show that all beams, except Beam G, had a major crack located between 20 to 25 inches from the ends. Calculations proved that for the static tests, Beam B failed in bond (Appendix D). For the dynamic tests, it is rather difficult to verify bond failure because of lack of information on dynamic reaction and increase in dynamic bond stress, etc. It can only be stated that the failure mechanism was similar to that of the static tests.

Beam G, subjected to a short-duration load, was the only one with no crack near the ends of the beam. This beam failed by compression of the concrete after the prestress steel had yielded.

Dynamic Resistance

To obtain the dynamic resistance, a single-degree-of-freedom system was used. Neglecting damping, the equivalent differential equation for a simply supported beam may be written as:

$$R = P(t) - m_e \ddot{y} \tag{18}$$

where R = resistance value

$P(t)$ = load

$m_e = 0.78m$ = mass of the single-degree-of-freedom system

$\ddot{y}$ = acceleration in g's

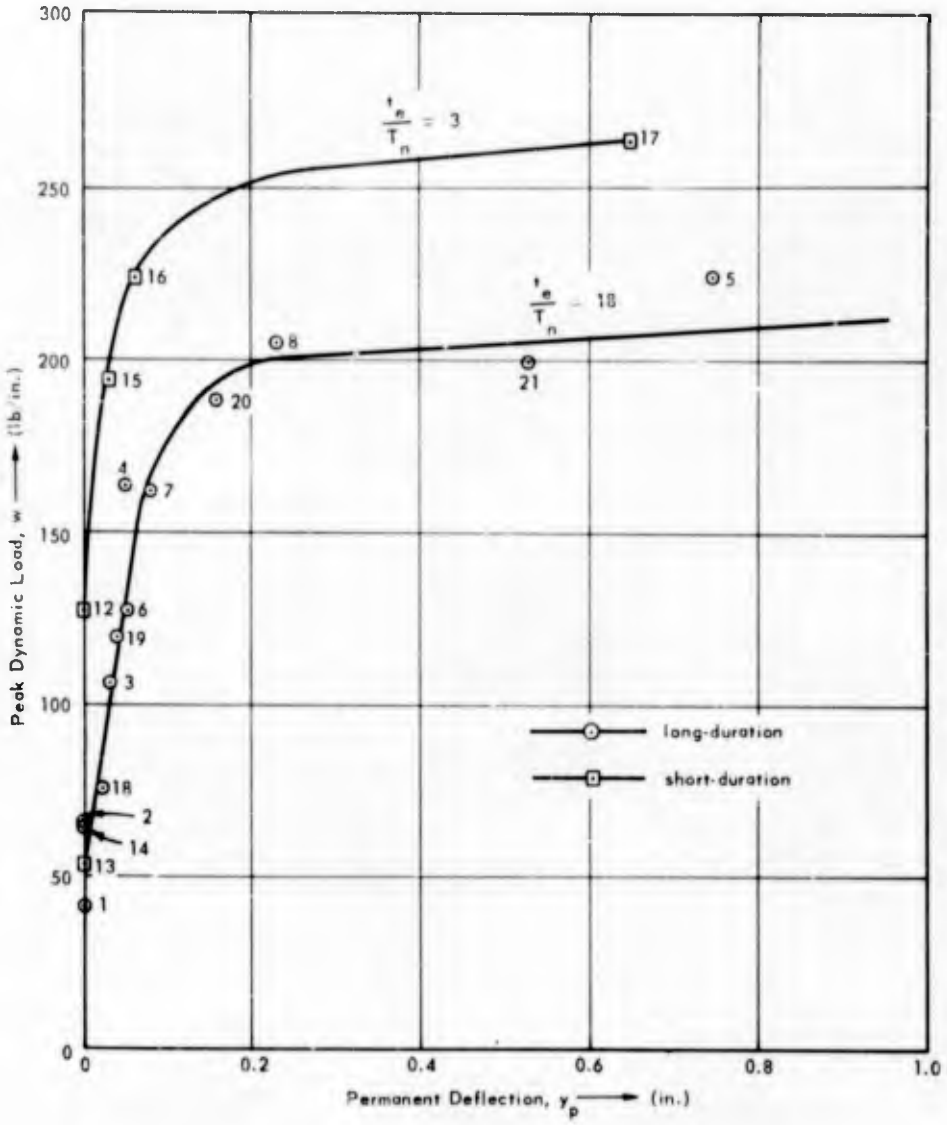

Figure 15. Plot of peak dynamic load versus permanent deflection.

For this experiment, a 100 g accelerometer was mounted at mid-span, and pressure cells were mounted about 2 inches above the top surface of the beam. With the load, deflection, and acceleration recorded on oscillograph, the dynamic resistance-deflection curves for Beams C and G were readily calculated. These results are shown in Figures 16 and 17; for comparison, the static resistance-deflection curve is plotted in dashed lines. In both cases the elastic slope for the dynamic resistance-deflection curve is seen to closely approximate the static resistance-deflection curve. This means that the static resistance value may be used in analytical computations instead of the dynamic resistance value if damping can be ignored. An example where this can be used is in calculating the dynamic shear, V, which is equal to 0.39 R + 0.11 P (Reference 10).

Experiments showed that the maximum dynamic reaction occurs at approximately the same time as the initial maximum deflection.[8] From Figure F-1 (Appendix F), the maximum deflection and time to maximum deflection for Beam A in test 2 were 0.30 inches and 20 milliseconds, respectively. Therefore from Figure 17, the static resistance is 19.50 kips. From Figure 13, which is an oscillogram for the same test, the average load at 20 milliseconds was calculated as 63 lb/linear inch or 9.83 kips. With this data, the dynamic reaction is calculated as

$$V = 0.39(19.50) + 0.11(9.83) = 8.68 \text{ kips}$$

The increase in reaction over the static reaction is $100(8.68 - 4.92) \div 4.92 = 77$ percent.

Response

From available response charts and methods, the maximum mid-span deflection was predicted for each peak load measured, and the results were compared with the experimental maximum deflection. Table VIII shows results obtained by using three different procedures to obtain maximum deflections for both long- and short-duration loads.

In the first method, response charts which account for plastic range slope were used.[11] These charts can be employed only when the beams are loaded into the plastic range and for long-duration loading. Since k_2/k_1 was rather large, the values were obtained by extending the curves of the lower k_2/k_1 values. Viscous damping of 2 percent was used.

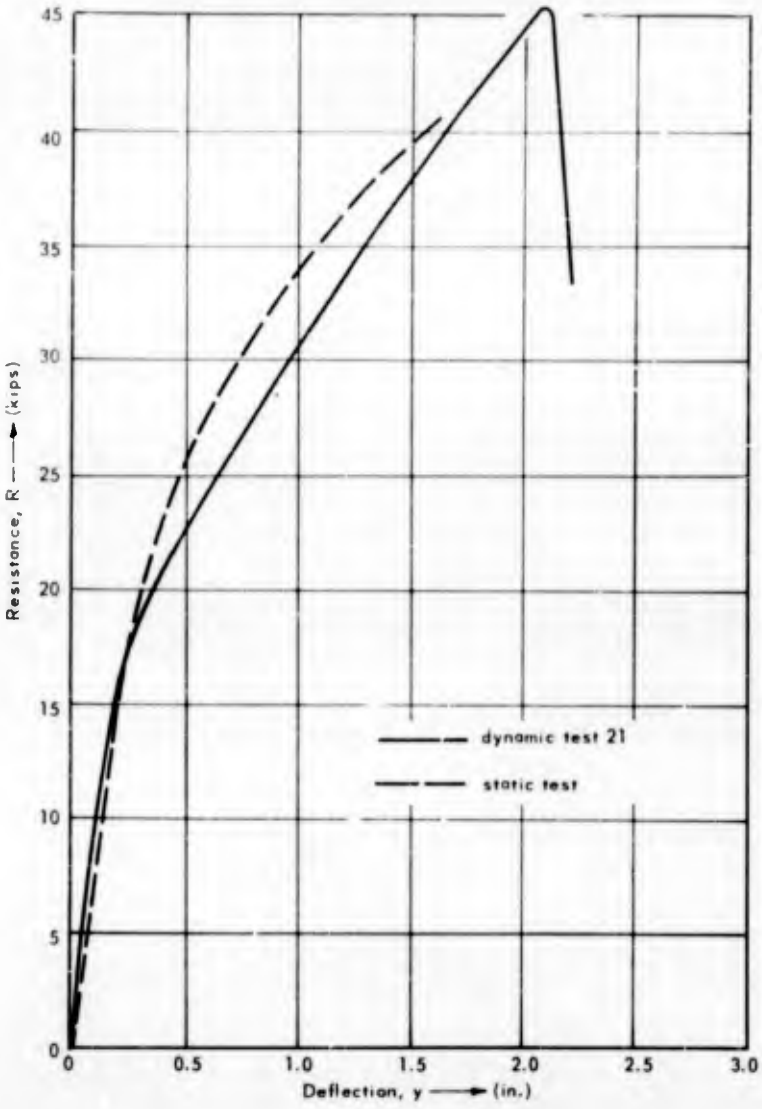

Figure 16. Resistance-deflection curve for Beam C.

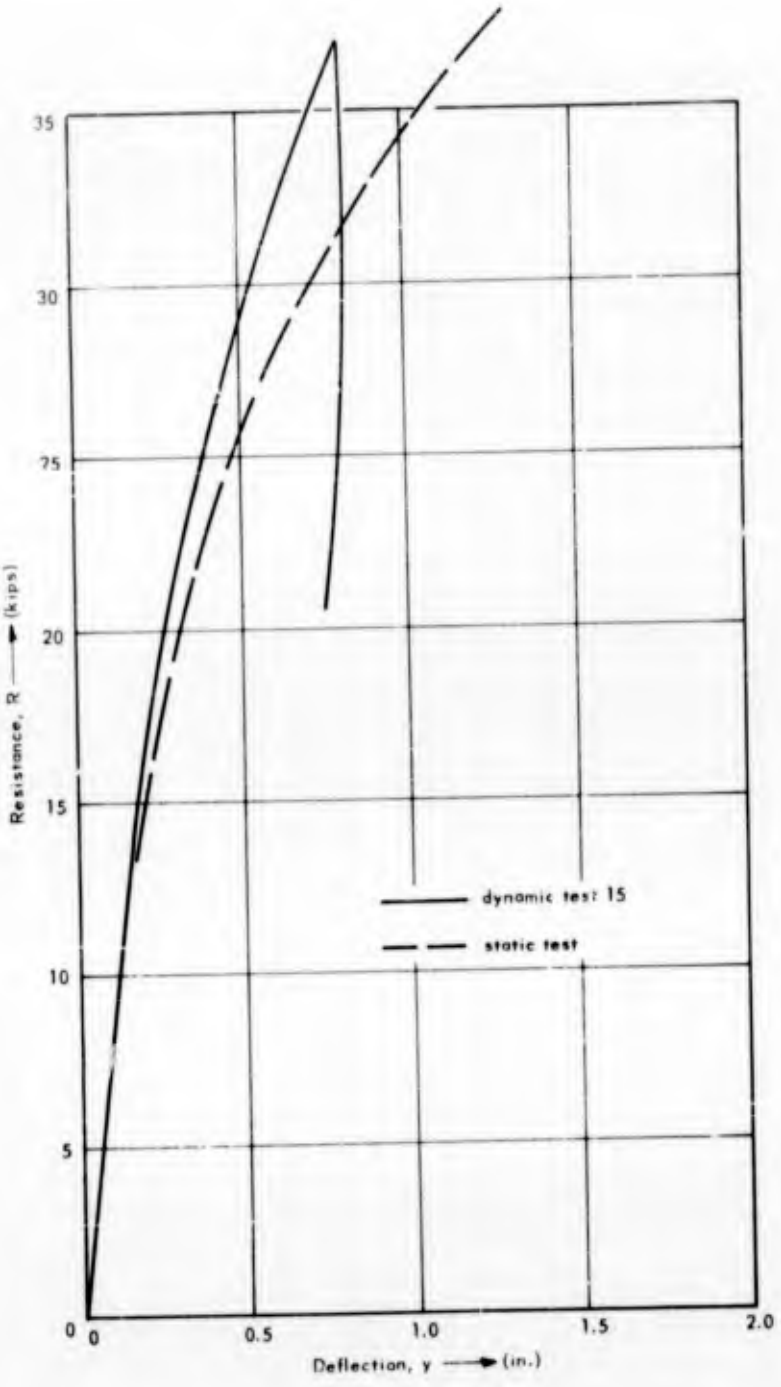

Figure 17. Resistance-deflection curve for Beam G.

Table VIII. Comparison of Theoretical versus Experimental Dynamic Responses

Static Properties

w_o = 160 lb/in. k_1 = 492 lb/in./in.

y_o = 0.325 in. k_2 = 83 lb/in./in.

Test No.	Experimental w_d (lb/in.)	Experimental y_m (in.)	Experimental $\frac{t_e}{T}$	Elastic (E) or Inelastic (P) Range	Dr. Thomson Design Charts[11] $\frac{w_d}{w_o}$	Dr. Thomson Design Charts[11] $\frac{y_m}{y_o}$	Dr. Thomson Design Charts[11] y_m (in.)	Corps of Engrs' Manual, 415[12] $\frac{y_m}{y_o}$	Corps of Engrs' Manual, 415[12] y_m (in.)	Equiv. Area Under Static Curve[3] A_e ++ (lb-in./in.)	Equiv. Area Under Static Curve[3] w_d (lb/in.)
1	41.1	0.15	18	E	0.26	*	*	0.43	0.14	5.75	38.4
2	65.9	0.30	18	E	0.41	*	*	0.70	0.23	18.75	62.5
3	106.4	0.54	18	P	0.67	*	*	1.65	0.54	51.62	95.8
4	163.9	1.18	18	P	1.02	3.5	1.14	+	+	186.50	158.0
5	223.6	2.70	18	P	1.40	7.0	2.28	+	+	—	—
6	127.4	0.90	18	P	0.80	2.02	0.66	+	+	134.00	148.9
7	162.0	1.45	18	P	1.01	3.40	1.10	+	+	249.50	172.1
8	204.9	1.65	18	P	1.28	5.7	1.85	+	+	301.00	182.4
9	223.9	2.87	18	P	1.40	7.0	2.28	+	+	—	—
12	127.8	0.37	3	E	0.80	**	**	1.55	0.50	**	**
13	53.8	0.14	3	E	0.34	**	**	0.60	0.19	**	**
14	64.8	0.17	3	E	0.40	**	**	0.64	0.21	**	**
15	194.4	0.82	3	P	1.21	**	**	+	+	**	**
16	223.0	1.52	3	P	1.39	**	**	+	+	**	**
17	264.4	2.65	3	P	1.55	**	**	+	+	**	**
18	75.3	0.36	18	E	0.47	*	*	0.68	0.22	29.25	81.2
19	118.8	0.74	18	P or E	0.74	1.85	0.60	2.0	0.65	90.75	122.6
20	178.3	1.75	13	P	1.18	4.90	1.59	+	+	353.00	201.7
21	196.5	2.21	18	P	1.24	5.40	1.75	+	+	—	—

* Not valid for elastic range

** Not valid for short-duration loads

\+ Not valid for inelastic range because $k_2 \neq 0$

++ A_e — area under static load-deflection curve

As a second procedure, the Corps of Engineers Manual EM 1110-345-415 was used.[12] The charts contained in this manual are suitable for both long- and short-duration loads because they take time into consideration. These charts are good for both fixed and simply supported beams. However, the charts do not cover resistance curves with plastic slopes other than zero. Hence, only the response from the elastic portion could be determined. The agreement (Table VIII) is very good when compared with experimental points.

In the third approach the Equivalent-Area-Under-Static-Curve Method[3] was used. The limitation of this method is that only long-duration response can be predicted and that the static resistance-deflection curve is identical to the dynamic resistance-deflection curve. This method consists mainly of picking a point on a static load-deflection curve, finding the area under the curve up to this point, and dividing this area by the deflection at the same point. The resulting value is the long-duration load which will have to be applied to obtain the static deflection. When the computed points of the last column in Table VIII are plotted, the resulting curve coincides almost precisely with the long-duration (t_e/T_n = 18) dynamic load-deflection curve (Figure 12) obtained from the experiment. Values for tests 5, 9, and 21 are not given because the static load-deflection curve extended only to a deflection of 1.5 inches.

FINDINGS AND CONCLUSIONS

This test program showed that pretensioned concrete beams have several advantages over ordinary reinforced concrete beams in blast-resistant construction: the recovery characteristics are excellent; negative deflection due to rebound is not a great factor except for very short-duration loads; and members are much smaller and lighter.

The major findings and conclusions are as follows:

1. In the elastic range, the initial maximum deflection for short- and long-duration loads can be predicted by using response charts based upon the single-degree-of-freedom system.

2. In the plastic range, the initial maximum deflection for a long-duration load can also be predicted by response charts if the damping factor and the static load-deflection relation are known.

3. For long-duration loads, the dynamic response factor in the elastic range is approximately 2.

4. Every beam, except for Beam G (which was subjected to a short-duration load), had a major crack located about 20 to 25 inches from the ends. Beams B, C, F, H, and K eventually failed by widening of the cracks since the 1/4-inch-diameter prestressing wires were not anchored at the ends.

5. The total prestress loss up to testing time was about 40,000 psi or 27.5 percent of the initial prestressing load.

6. Permanent deflections are not produced by dynamic loads less than about 85 percent of the failure load.

7. There was no tensile stress introduced in the top fiber at any time for either long- or short-duration dynamic loadings.

8. The ultimate static load and deflection can be predicted by using the moment-rotation diagram.

ACKNOWLEDGMENT

The author wishes to acknowledge the contributions of Messrs. Sterling L. Bugg, Jay R. Allgood, and Warren A. Shaw of NCEL, who reviewed the report and made many helpful suggestions, and of Mr. Robert L. Henry, also of NCEL, who prepared the beams for testing.

REFERENCES

1. Janney, Jack R. "Nature of Bond in Pre-tensioned Prestressed Concrete." ACI Journal, Vol. 25, No. 9 (May 1954).

2. Hanson, Norman W., and Paul H. Kaar. "Flexural Bond Tests of Pretensioned Prestressed Beams." ACI Journal, Vol. 55, No. 7 (January 1959).

3. Naval Civil Engineering Laboratory (NCEL). Technical Report R-116, Blast Load Tests on Post-Tensioned Concrete Beams, by H. T. Miyamoto and J. R. Allgood. Port Hueneme, California, 29 May 1961.

4. Shaw, W. A., and J. R. Allgood. "An Atomic Blast Simulator." SESA Proceedings, Vol. 17, No. 1 (1959).

5. NCEL. Technical Report R-086, Blast Loading of 15-Foot R/C Beams, by J. R. Allgood, S. K. Takahashi, and W. A. Shaw. Port Hueneme, California, 9 January 1961.

6. NCEL. Technical Report R-148, Blast Loading of 8-Foot Aluminum Beams, by S. K. Takahashi and D. F. Green. Port Hueneme, California, 9 June 1961.

7. Swihart, G. R., J. R. Allgood, and W. A. Shaw. "Resistance of Reinforced Concrete Beams." Proceedings of ASCE, Vol. 85, No. ST 1, Part 1 (January 1959).

8. NCEL. Technical Memorandum M-130, Elasto-Plastic Response of Beams to Dynamic Loads, by J. R. Allgood and W. A. Shaw. Port Hueneme, California, 3 March 1958.

9. Jacobsen, L. S., and R. S. Ayre. Engineering Vibrations. McGraw-Hill Book Co., Inc., New York, 1958.

10. U. S. Army, Manuals-Corp of Engineers. EM 1110-345-416, Design of Structures to Resist the Effects of Atomic Weapons, Structural Elements Subjected to Dynamic Loads. 15 March 1957.

11. University of California, Department of Engineering. Report No. 57-53 (55-52 Revised), Dynamic Response of Single Span Beams in the Plastic Region, by W. T. Thomson. Los Angeles, California, June 1957.

12. U. S. Army, Manuals-Corp of Engineers. EM 1110-345-415, Design of Structures to Resist the Effects of Atomic Weapons, Principles of Dynamic Analysis and Design. 15 March 1957.

13. ACI-ASCE Joint Committee 323. "Tentative Design Recommendations for Prestressed Concrete." ACI Journal, Vol. 29, No. 7 (January 1958).

14. Timoshenko, S., and D. H. Young. Vibration Problems in Engineering. D. Van Nostrand Company, Inc., New York, 1956.

15. Lin, T. Y. Design of Prestressed Concrete Structures. John Wiley and Sons, New York, 1958.

NOMENCLATURE

A	area
A_1	area of plastic portion of unit rotation diagram
A_2	area of elastic portion of M/EI diagram
A_e	area of steel
A_{ss}	total area of high strength steel below the neutral axis
A'_s	total area of compressive mild steel above the neutral axis
A'_{ss}	total area of high strength steel above the neutral axis
a	distance from the top of the beam to the neutral axis at mid-span
b	width of beam
C_c	total force in concrete above the neutral axis
C_i	initial total compressive force in mild steel
C_s	total compressive force in mild steel
C'_s	total force in prestress steel above the neutral axis
C'_{si}	initial total force in prestress steel above the neutral axis
c	distance from the neutral axis to the extreme fiber
d	distance from top of beam to c.g. of prestress steel
d'	distance from top of beam to c.g. of compressive mild steel
d'_s	distance from top of beam to c.g. of prestress steel above the neutral axis
E_c	modulus of elasticity of concrete
E_s	Young's modulus of elasticity of reinforcing mild steel

E_{ss}	Young's modulus of elasticity of prestress steel
E'_s	plastic modulus of mild steel
E'_{ss}	plastic modulus of prestress steel
f	fiber stress
f'_c	ultimate concrete compressive stress
f_p	stress at proportional limit
f_{ssi}	stress in prestress steel below neutral axis prior to test
f'_{ssi}	stress in prestress steel above neutral axis prior to test
f'_t	extreme fiber tensile cracking stress of concrete
f_y	yield point stress of mild steel
f_{yp}	yield point stress of prestress steel
g	acceleration due to gravity
h	total depth of beam
I	moment of inertia about the x-x axis
k_1	stiffness of beam in the elastic range
k_2	stiffness of beam in the plastic range
$k_2 a$	distance from the compressive fiber to the location of the resultant concrete compressive force
k_3	$(3,900 + 0.35 f'_c)/[3,000 + 0.82 f'_c - (f'^2_c/26,000)]$
L	clear span length of beam
M	moment
M_c	cracking moment

M_d	dead load moment
M_u	ultimate moment
m	mass of pretensioned beam
m	a factor when multiplied by "ba" will give the total concrete compressive force if b is the width of the beam
m_e	equivalent mass
o	perimeter of a prestressed steel wire
P	load
P_m	peak dynamic load
P (t)	dynamic load varying with time
R	dynamic resistance
S	section modulus
T	total duration of load
T_i	total tensile force in the prestress steel below the neutral axis
T_n	natural period of vibration
t_e	effective duration of load
u	bond strength
V	dynamic shear
W	total weight of beam
w_d	dynamic load per unit length of beam
w_{dl}	weight of beam per unit length of beam
w_o	yield load per unit length of beam

w_s	static load per unit length of beam
w_u	ultimate load per unit length of beam
$\bar{x}$	distance to center of gravity of parabolic area
y	deflection
$\ddot{y}$	acceleration of mid-span of beam
y_m	initial maximum deflection
y_o	yield deflection at mid-span
y_s	static deflection
α	plastic hinge coefficient
ϵ_c	concrete strain
ϵ_{ci}^{B}	concrete strain in the lower fiber due to pretensioning and dead load at time of test
ϵ_{ci}^{T}	concrete strain in the top fiber due to pretensioning and dead load at time of test
ϵ_o	unit strain at maximum stress f''_c, inch/inch
ϵ_p	strain at proportional limit
ϵ_s	prestress steel strain
ϵ'_{ssi}	increase in prestress steel strain below the neutral axis
ϵ''_{ssi}	increase in prestress steel strain above the neutral axis
ϵ_u	ultimate concrete strain
ϵ_{yp}	yield strain
θ	unit rotation

Appendix A

APPLICATION OF THEORY FOR STATIC LOADS

In order to compare the theoretical computation with experimental values, Beam H was chosen because bond failure occurred at a higher load than Beams B and K. The properties of Beam H are:

$A_{ss} = 0.589 \text{ inch}^2$ $\quad E_s = E_{ss} = 28.8 \times 10^3 \text{ ksi}$

$A'_{ss} = 0.098 \text{ inch}^2$ $\quad E'_{ss} = 2.55 \times 10^3 \text{ ksi}$

$A'_s = 0.392 \text{ inch}^2$ $\quad f_{ssi} = f'_{ssi} = 103.9 \text{ ksi}$

$h = 10 \text{ inches}$ $\quad f_{yp} = 217.9 \text{ ksi}$

$b = 7.75 \text{ inches}$ $\quad f_y = 50.9 \text{ ksi}$

$L = 156 \text{ inches}$ $\quad f'_c = 8.30 \text{ ksi}$

$d = 7.55 \text{ inches}$ $\quad E_c = 1.8 \times 10^3 + 0.46 f'_c = 5.62 \times 10^3 \text{ ksi}$

$d'_s = 1.41 \text{ inches}$ $\quad f'_s = 13.35 \text{ ksi}$

$d' = 1.62 \text{ inches}$ $\quad I_{x-x} = 689 \text{ inches}^4$ (uncracked section)

$n = E_s/E_c = 5.12$

$$\epsilon_u = 0.004 - \frac{f'_c}{6.5 \times 10^6} = 0.003 \frac{\text{in.}}{\text{in.}} \qquad w_{dl} = 6.90 \frac{\text{lb}}{\text{in.}}$$

$$k_3 = \frac{3,900 + 0.35(8,300)}{3,000 + 0.82(8,300) - \frac{8,300^2}{26,000}} = 0.952$$

$$f'_c = 0.952(8,300) = 7,890 \text{ psi}$$

$$0.85 f'_c = 6,710$$

$$\epsilon_o = \frac{2 f'_c}{E_c} = \frac{2 (7.890)}{5.62 \times 10^3} = 0.002805 \frac{\text{in.}}{\text{in.}}$$

Cracking load is designated as that load which causes the concrete at mid-span to crack initially due to bending forces.[13]

$$f'_t = 7.5 \sqrt{f'_c} = 7.5 \sqrt{8,300} = 683 \text{ psi}$$

The initial prestress compression values are 0 at top and 2,000 psi at bottom fibers of beam.

$$M_{cr} = M_i + f'_t S = (2,000 + 683)(138) = 370,200 \text{ in.-lb}$$

$$w_{cr} = \frac{8 M_{cr}}{L^2} - w_{dl} = \frac{8 (370,200)}{148^2} - 6.90 = 128.1 \frac{\text{lb}}{\text{in.}}$$

$$\epsilon_{cr} = \frac{M_{cr}}{E_c S} = \frac{370,200}{(5.62 \times 10^6)(138)} = 477 \frac{\mu \text{in.}}{\text{in.}}$$

$$E_c I = 3.87 \times 10^9 \text{ lb-in.}^2$$

$$y_{cr} = \frac{5 w L^4}{384 E_c I} = \frac{5 (128.1)(148)^2}{384 (3.87 \times 10^9)} = 0.207 \text{ inch}$$

Working load is designated as that load which causes the concrete at mid-span to have a compressive stress of zero at the lower fiber and 2,000 psi at the upper fiber.

$$M_w = 2,000\,(138) = 276,000 \text{ in.-lb}$$

$$w_w = \frac{8\,(276,000)}{148^2} = 101\ \frac{\text{lb}}{\text{in.}}$$

$$y = \frac{5\,(101)\,(148)^4}{384\,(3.87 \times 10^9)} = 0.163 \text{ inch}$$

For the post-cracking range, let $\epsilon_c = 0.001\ \frac{\text{in.}}{\text{in.}}$ which is less than ϵ_o.

$$f_c = 7.890\left[2\left(\frac{1,000}{2,805}\right) - \left(\frac{1,000}{2,805}\right)^2\right] = 4.62 \text{ ksi}$$

$$m = \frac{1}{3\,(1,000)}\left[1,000\,(15.780 + 4.62) - 4.62\,(2,805)\right] = 2.48 \text{ ksi}$$

$$T = 0.585\left[103.9 + (1 \times 10^{-3})\left(\frac{7.55 - a}{a}\right)(28.8 \times 10^3)\right]$$

$$C_s' = 0.098\left[103.9 - (1 \times 10^{-3})\left(\frac{a - 1.41}{a}\right)(28.8 \times 10^3)\right]$$

$$C_s = 0.392\left[(-1 \times 10^{-3})\left(\frac{a - 1.62}{a}\right)(28.8 \times 10^3) - 13.35\right]$$

$$C = 248\,(7.75)\,a$$

Summation of these forces must add up to zero:

$$T + C'_s + C_s + C = 0$$

a is found to be equal to 3.85 inches.

$$T = 7,740 \text{ kips}, \qquad \frac{T}{A_{ss}} = 131.2 \text{ ksi} < f_{yp}$$

$$C'_s = 8.38 \text{ kips}, \qquad \frac{C'_s}{A'_{ss}} = 85.5 \text{ ksi} < f_{yp}$$

$$C_s = -11.76 \text{ kips}, \qquad \frac{C_s}{A'_s} = 30.0 \text{ ksi} < f_y$$

$$C = -74.00 \text{ kips}, \qquad \epsilon_c < \epsilon_o$$

The moment at mid-span can be found from Equation 11 (in text):

$$M_n = C(d - k_2 a) + C_s(d - d') + C'_s(d - d'_s)$$

From Reference 7

$$k_2 a = a - \bar{Y} = a - a \left[\frac{\frac{f''_c + f_c}{4} + \frac{\epsilon_o}{\epsilon_c}\left(\frac{f''_c - f_c}{6}\right) - \frac{f_c \epsilon_o^2}{12 \epsilon_c^2}}{\frac{2f''_c + f_c}{3} - \frac{f_c \epsilon_o}{3\epsilon_c}} \right]$$

$$k_2 a = 1.31 \text{ inches}$$

M_1 is then found to be 479.3 kip-inches.

$$w = \frac{8 M_1}{L^2} = 157 \frac{lb}{in.}$$

Increase in moment after cracking:

$$M_{pc} = 479.3 - M_{cr} = 109.1 \text{ kip-in.}, \quad I = 188.8 \text{ in.}^4$$

By moment-area method,

$$y_{pc} = \frac{\frac{2}{3}(78)(109.1)}{(5.62 \times 10^3)(188.8)} \times \frac{5}{8}(78) = 0.261 \text{ in.}$$

Total deflection, $y_1 = y_{cr} + 0.26 = 0.47$ inch. Letting $\epsilon_c = 0.002 \frac{in.}{in.}$

$$a = 3.06 \text{ in.}, \qquad f_c = 7,230 \text{ psi}$$

$$T = 110.9 \text{ kips}, \qquad \frac{T}{A_{ss}} = 188 \text{ ksi} < f_{yp}$$

$$C'_s = 7.12 \text{ kips}, \qquad \frac{C'_s}{A'_{ss}} = 72.6 \text{ ksi} < f_{yp}$$

$$C_s = -15.68 \text{ kips}, \qquad \frac{C_s}{A'_s} = 39.9 \text{ ksi} < f_y$$

$$C_c = -102.0 \text{ kips}, \qquad \epsilon_c < \epsilon_o$$

$$M_2 = 707.1 \text{ kip-in.}$$

$M_{pc} = 707.1 - M_{cr} = 336.9$ kip-in., $\quad I = 134.8$ in.^{4}

$w = 232 \frac{lb}{in.}$, $\quad y_{pc} = \frac{0.451 M_{pc}}{I} = 1.127$ in.

$y_2 = y_{cr} + 1.13 = 1.34$ in.

By extending the curve in Figure A-1, the tensile prestress steel yields at $\epsilon_c = 0.0052$ in./in. The values calculated at the strain are:

$a = 2.99$ in., $\quad f_c = 7,800$ psi

$T = 126.2$ kips, $\quad \frac{T}{A_{ss}} = 215$ ksi $\cong f_{yp}$

$C'_s = 6.41$ kips, $\quad \frac{C'_s}{A'_{ss}} = 65.4$ ksi $< f_{yp}$

$C_s = -18.26$ kips, $\quad \frac{C_s}{A'_s} = 46.6$ ksi $< f_y$

$C_c = -114.50$ kips, $\quad \epsilon_c < \epsilon_o$

$M_3 = 807.6$ kip-in.

$M_{pc} = 807.6 - M_{cr} = 437.4$ kip-in., $\quad I = 131.7$ in.^{4}

$w = 265 \frac{lb}{in.}$, $\quad y_{pc} = \frac{0.451 M_{pc}}{I} = 1.50$ in.

$y_3 = y_{cr} + 1.50 = 1.71$ in.

Initial yielding is taken at this load and deflection.

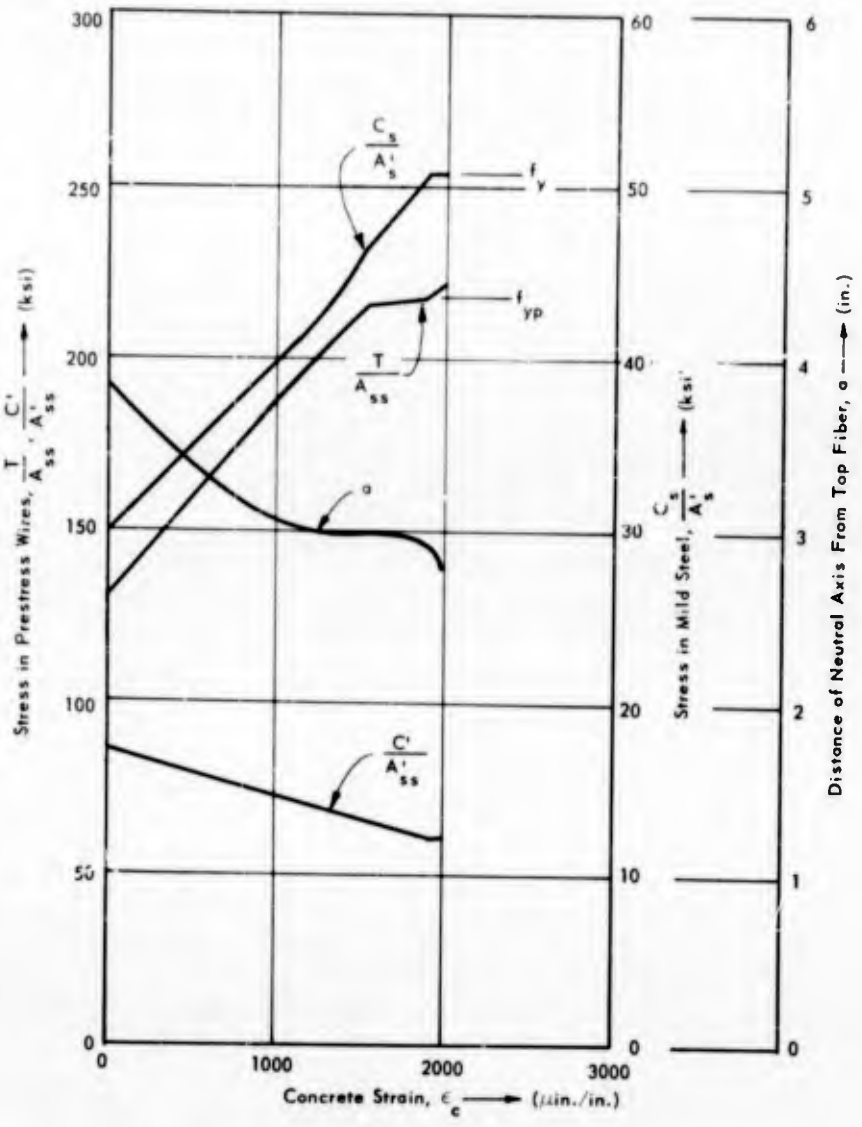

Figure A-1. Plot of concrete strain versus stresses in steel and location of the neutral axis.

Again by interpolation, the mild steel is seen to yield at

$$\epsilon_c = 0.0029 \frac{\text{in.}}{\text{in.}}$$

Then m is found by using Equation 9 in the text. This time the T value is calculated from Equation 2 in the text. Since $\epsilon_c > \epsilon_o$,

$$k_2 a = a - \frac{\frac{a}{12}\left[2(f''_c + 2f_c) + \frac{2\epsilon_o}{\epsilon_c}(f''_c - f_c) + \frac{\epsilon_o^2}{\epsilon_c^2}(f''_c - 2f_c)\right]}{\frac{1}{2\epsilon_c}\left[\frac{f''_c(3\epsilon_c + \epsilon_o)}{3} + f_c(\epsilon_c - \epsilon_o)\right]}$$

$a = 2.91$ in., $\quad f_c = 7{,}290$ psi

$T = 128.9$ kips, $\quad \frac{T}{A_{ss}} = 218.5$ ksi

$C'_s = 5.95$ kips, $\quad \frac{C'_s}{A'_{ss}} = 60.7$ ksi

$C_s = -19.78$ kips, $\quad \frac{C_s}{A'_s} = 50.9$ ksi $= f_y$

$C_c = -114.80$ kips, $\quad \epsilon_c > \epsilon_o$

$M_3 = 819.5$ kip-in.

$M_{pc} = 819.5 - M_{cr} = 449.3$ kip-in.

$w = 269 \frac{\text{lb}}{\text{in.}}$

The ordinary methods cannot be used for computing the deflection for this load because the beam has yielded. Therefore the unit rotation diagram[7] is used, with w_o = 265 lb/in. The deflection is then calculated as 2.06 inches. At this load, the tensile prestress steel has yielded, and the compressive mild steel has just reached its yield point.

When ϵ_c = 0.003 in./in., the concrete has reached its ultimate strain. In the range ϵ_c = 2,520 to 3,000 μin./in., Equation 6 is used to compute C_s.

$$C_c = abf''_c \left(0.925 - 0.258 \frac{\epsilon_o}{\epsilon_u}\right)$$

and

$$f_c = 0.85 f''_c$$

The values calculated are then

a = 2.74 in., $\quad f_c$ = 6,710 psi

T = 130 kips, $\quad \frac{T}{A_{ss}}$ = 221 ksi > f_{yp}

C'_s = 6.06 kips, $\quad \frac{C'_s}{A'_{ss}}$ = 61.9 ksi < f_{yp}

C_s = -19.95 kips, $\quad \frac{C_s}{A'_s}$ = 50.9 ksi = f_y

C_c = 116 kips

M_4 = 841.9 kip-in.

M_{pc} = 841.9 - M_{cr} = 471.7 kip-in., $\quad I$ = 113.38 in.^{4}

$w = 277 \frac{\text{lb}}{\text{in.}}$

y_4 = 2.38 in.

Therefore, the beam fails by crushing of the concrete — assuming no bond slippage. The theoretical values are summarized in Table IX.

Table IX. Summary of Theoretical Values for Beam H

ϵ_c (μin./in.)	1,000	2,000	2,520	2,900	3,000
a (in.)	3.85	3.06	2.99	2.99	2.74
M (kip-in.)	479.3	707.1	807.6	819.5	841.9
w (lb/in.)	157	232	265	269	277
y (in.)	0.47	1.34	1.71	2.06	2.38
T/A_{ss} (ksi)	131.2	188	215	219	221
C_s'/A_{ss}' (ksi)	85.5	72.6	65.4	60.7	61.9
C_s/A_s' (ksi)	30.0	39.9	46.6	50.9	50.9
f_c (ksi)	4.62	7.23	7.80	7.29	6.71

The values T/A_{ss}, C_s'/A_{ss}', C_s/A_s', and a are plotted in Figure A-1 and the values w and y_n are plotted in Figure A-2. The experimental static load-deflection curve is also shown in dotted lines for comparison.

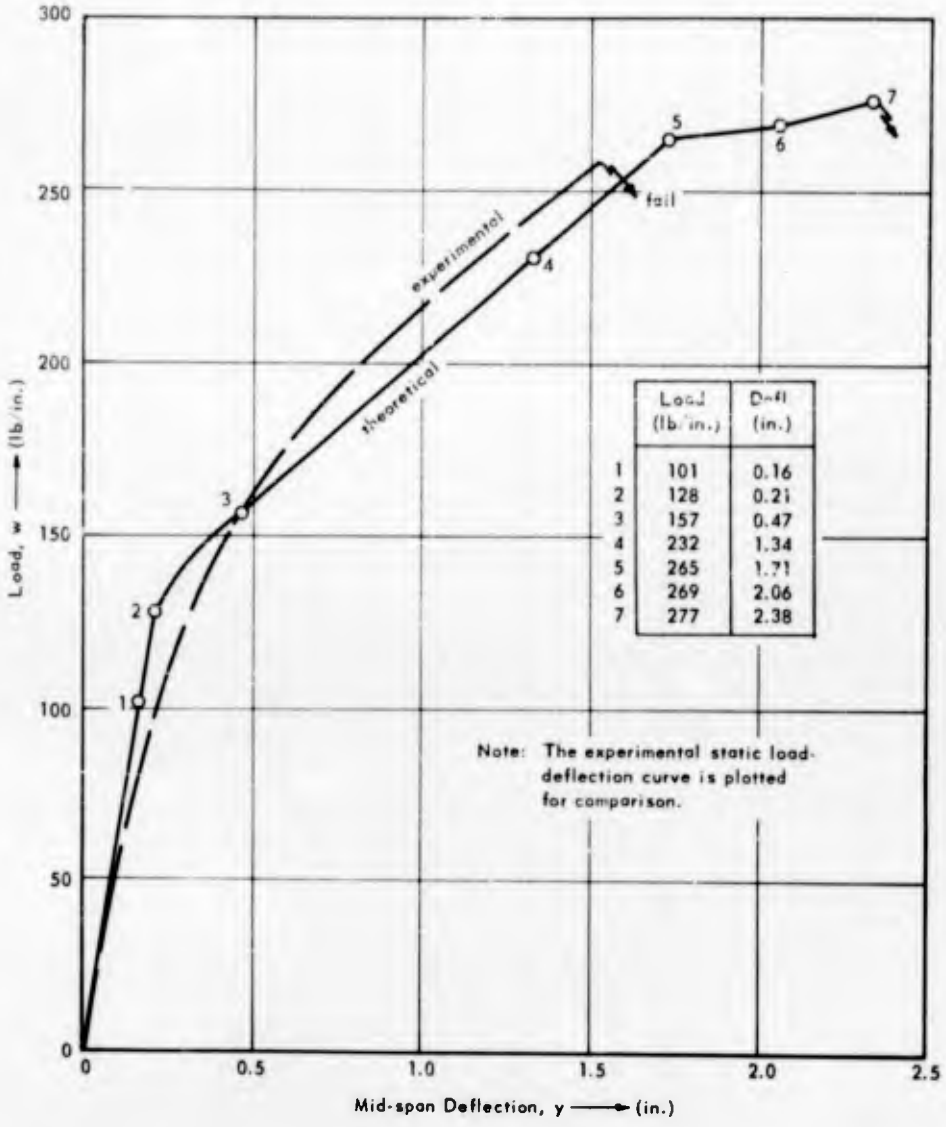

Figure A-2. Plot of theoretical static load-deflection curve for Beam H.

Appendix B

DIFFERENTIAL EQUATION SOLUTION APPLIED TO DYNAMIC RESPONSE

The response of a simply supported beam, such as shown in Figure B-1A, subjected to a triangular pulse load was shown previously as:

$$y = \frac{P_o}{k}\left[1 + \frac{e^{-\zeta\omega t}\left(\frac{1}{\omega t_e} - \zeta - \frac{2\zeta^2}{\omega t_e}\right)\sin\left(\omega\sqrt{1-\zeta^2}\,t\right)}{\sqrt{1-\zeta^2}} - e^{-\zeta\omega t}\left(\frac{2\zeta}{\omega t_e} + 1\right)\cos\left(\omega\sqrt{1-\zeta^2}\,t\right) - \frac{t}{t_e} + \frac{2\zeta}{\omega t_e}\right] \qquad \text{(B1)}$$

The equivalent spring-mass system is shown in Figure B-1B. In Figure B-2, the oscillogram record for dynamic test 2, Beam A, is reproduced. The pressure or load trace is idealized into a triangular pulse which decreases to zero at time equal to 603 milliseconds. The peak total load (P_o), at time-equal-to-zero, is calculated as 10, 125 pounds.

From Figure B-2, the natural period of the beam obtained from the oscillation of the acceleration trace is

$$T_n = 35 \text{ msec/cycle}$$

The natural circular frequency may then be calculated as

$$\omega = \frac{2\pi}{T_n} = 0.180 \text{ rad/msec or } 180 \text{ rad/sec}$$

The spring constant is calculated as

$$k = m_e\omega^2 = \frac{0.78\,(1,021)\,(180)^2}{386.4} = 66,777 \text{ lb/in.}$$

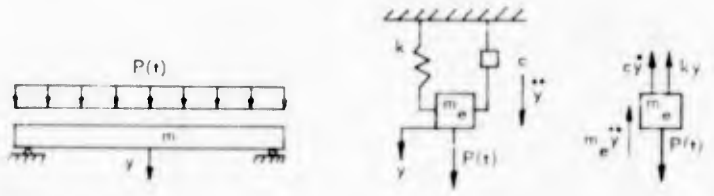

A. The beam B. Equivalent system

Figure B-1. The beam and its equivalent single-degree-of-freedom system.

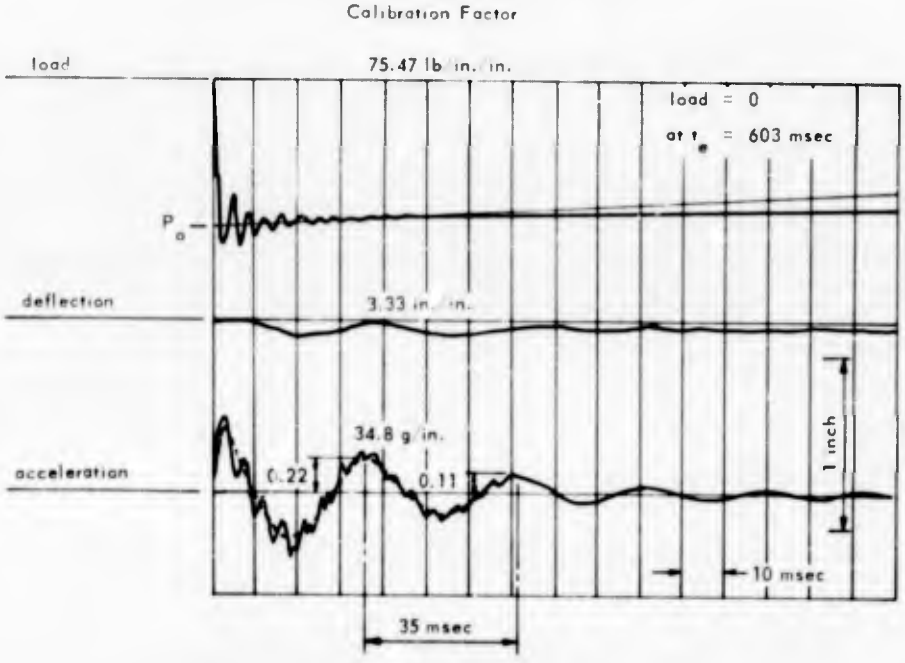

Figure B-2. Oscillogram for Beam A, dynamic test 2.

The spring constant, k, may be calculated theoretically by first determining the natural period of vibration,[14]

$$T'_n = \frac{2L^2}{\pi n^2}\sqrt{\frac{A\gamma}{EIg}}$$

where L = clear span length of beam, inch

n = mode of vibration

A = cross-sectional area, $inch^2$

γ = weight of material per unit volume, $lb/in.^3$

E = modulus of elasticity of concrete, $lb/in.^2$

I = moment of inertia, $inch^4$

g = acceleration due to gravity, $in./sec^2$

$$T'_n = \frac{2(148)^2}{\pi(1)^2}\sqrt{\frac{7.75(10)\,\frac{1,021}{7.75(10)(148)}}{(4.7\times 10^6)\,\frac{7.75(10^3)}{12}(386)}} = 0.0338 \text{ sec} = 33.8 \text{ msec/cycle}$$

The natural circular frequency may then be calculated as

$$\omega' = \frac{2\pi}{T'_n} = 185.89 \text{ rad/sec}$$

from which the theoretical stiffness is found as

$$k = m_e\omega^2 = 71,000 \text{ lb/in.}$$

The experimental values will be used in solving the differential equation.

The logarithmic decrement for one cycle is (see Figure B-2)

$$\delta = \ln\left(\frac{x_o}{x_1}\right) = \ln\left(\frac{0.22}{0.11}\right) = 0.6932$$

The damping factor is then

$$\zeta = \sqrt{\frac{\delta^2}{\delta^2 + 4\pi^2}} = 0.11 \text{ or } 11 \text{ percent}$$

Inserting the numerical values from test 2, Beam A, in Equation B-1,

$$y = 0.15162\left[1.00203 - \frac{0.10101}{0.99394}\, e^{-19.8t} \sin(178.90920\,t)\right.$$

$$\left. - 1.00203\, e^{-19.8t} \cos(178.90920\,t) - 1.65837\,t\right] \qquad \text{(B2)}$$

Taking time increments of 5 milliseconds, the corresponding deflections were calculated from Equation B2 and plotted in Figure B-3. The experimental deflection-time curve for Beam A, test 2, in Figure F-1 is replotted in Figure B-3 for comparison.

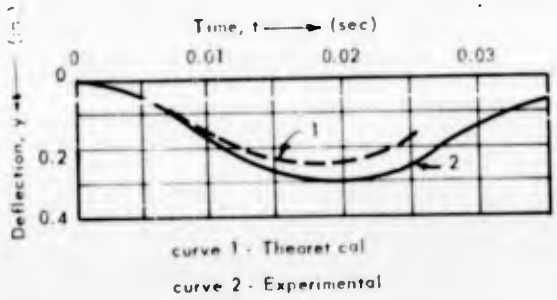

Figure B-3. Comparison of theoretical and experimental deflection for Beam A, dynamic test 2.

Appendix C

PHOTOS OF BEAMS

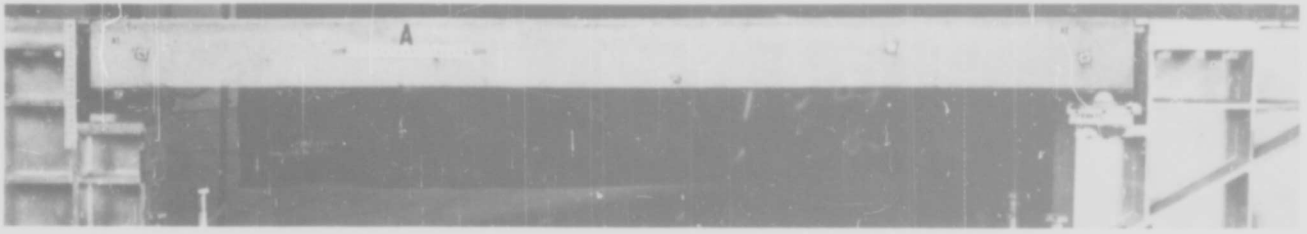

Figure C-1. Beam A after a dynamic load of 224 lb/linear inch.

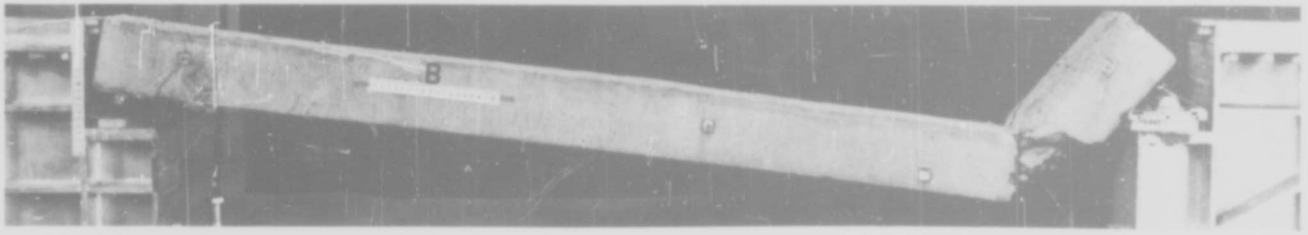

Figure C-2. Beam B after a static load of 211 lb/linear inch.

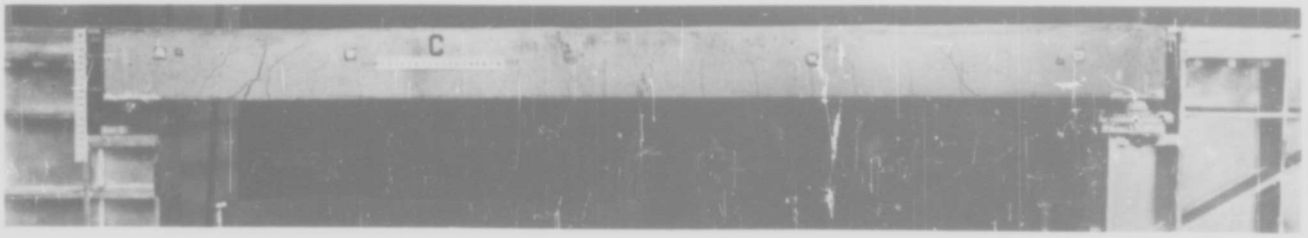

Figure C-3. Beam C cfter a dynamic load of 199 lb/linear inch.

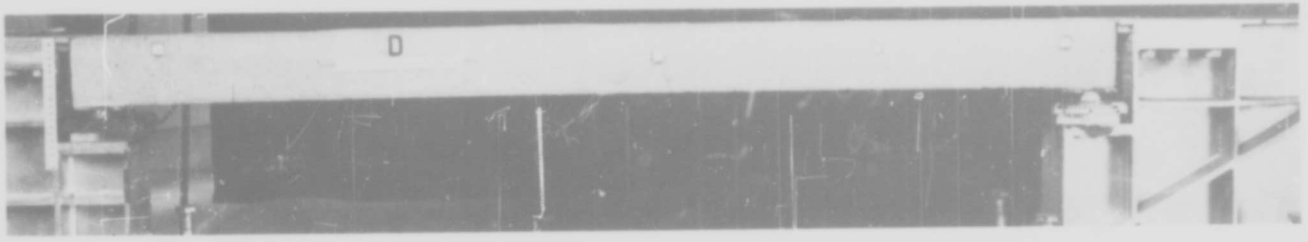

Figure C-4. Beam D after a dynamic load of 205 lb/linear inch.

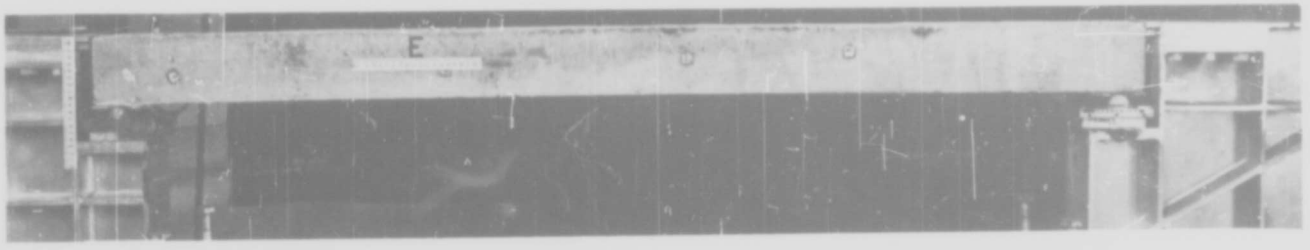

Figure C-5. Beam E after a dynamic load of 162 lb/linear inch.

Figure C-6. Beam F after a dynamic load of 224 lb/linear inch.

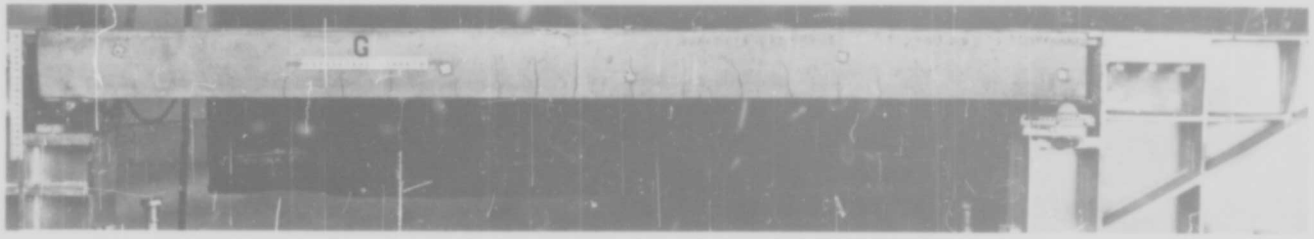

Figure C-7. Beam G after a dynamic load of 264 lb/linear inch.

Figure C-8. Beam H after a static load of 260 lb/linear inch.

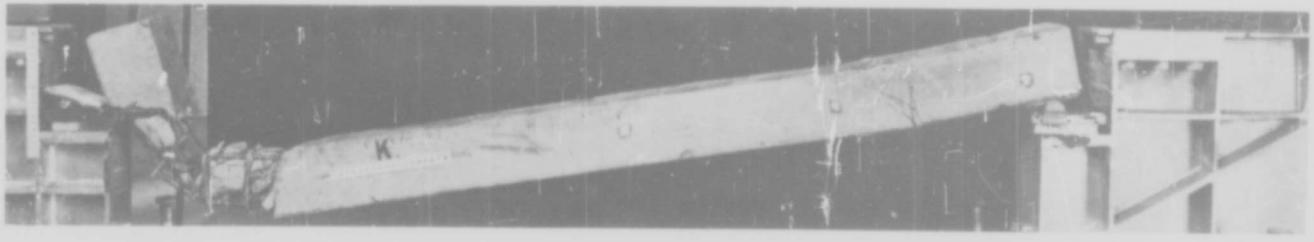

Figure C-9. Beam K after a static load of 268 lb/linear inch.

Appendix D

MODE OF FAILURE OF BEAM B (MAXIMUM STATIC LOAD OF 219 LB/LINEAR INCH)

The locations of the cracks in the concrete are shown in Figure D-1.

The initial prestress steel strains measured are

$$\epsilon_1 = 3,630\ \mu\text{in./in.}$$

$$\epsilon_3 = 3,490\ \mu\text{in./in.}$$

The initial stresses are

$$f_1 = 28.8 \times \epsilon_1 = 104,300\ \text{psi}$$

$$f_3 = 28.8 \times \epsilon_3 = 100,500\ \text{psi}$$

$$\text{Avg } f = 102,400\ \text{psi}$$

The strains at ultimate load are

$$\epsilon_1 = 2,490 + 3,630 = 6,120\ \mu\text{in./in.}$$

$$\epsilon_3 = 1,540 + 3,490 = 5,030\ \mu\text{in./in.}$$

which is less than the 0.2-percent yield value of 7,550 μin./in.

The extreme fiber stress of concrete at cracking load should be[13]:

$$f'_t = 7.5\sqrt{f'_c} = 7.5\sqrt{7,290} = 640\ \text{psi}$$

Figure D-1. Failure mode of Beam B.

Initial concrete stress is

$$f_{ci} = \frac{2 f_s A_s}{bd} = \frac{2 (102,400) (0.7)}{7.75 (10)} = 1,850 \text{ psi}$$

Determine the limit of flexural cracks by first obtaining the cracking moment, M_c:

$$M_c = (f_{ci} + f'_t) (S) = (1,850 + 640) (129) = 321,000 \text{ in.-lb}$$

The distance, x, of the last crack from one end of the beam is then obtained by equating the external and internal moment:

$$Vx - \frac{wx^2}{2} = M_c$$

or

$$16,200x - 219 \frac{x^2}{2} = 321,000$$

$$x = 23.6 \text{ inches from the support}$$

Check the diagonal tension stresses at 25 inches from the support and 2 inches from the bottom of the beam. The shear at 25 inches from the support, V_{25}, is

$$V_{25} = \frac{wL}{2} - 25w = \frac{219 (148)}{2} - 25 (219) = 10,725 \text{ lb}$$

The moment at the same location is

$$M_{25} = 25V - \frac{w (25)^2}{2} = 25 (16,200) - \frac{219 (25)^2}{2} = 336,600 \text{ in.-lb}$$

Calculating the statical moment, Q_s, of an area 2 inches from the bottom of the beam,

$$Q_s = 2\,(7.75)\,(4) = 62 \text{ in.}^3$$

the unit shear, v_2, at 25 inches from the support is calculated as

$$v_2 = \frac{V_{25} Q_s}{Ib} = \frac{10,725\,(62)}{645\,(7.75)} = 133 \text{ psi}$$

The corresponding fiber stress, f_2, is then

$$f_2 = \frac{M_{25} y}{I} - 0.7 f_c = \frac{336,600\,(3)}{645} - 0.7\,(1,850) = 270 \text{ psi}$$

By drawing the Mohr circle, the values of the principal compressive and tensile stresses were determined to be 53 psi and 327 psi respectively.[15] Since 327 psi is about one-half of the cracking stress, the beam is not likely to fail by shear and diagonal tension.

In investigating bond, for a 0.197-inch-diameter clean wire, the full prestress is obtained at a distance, L', of 20 inches from the free end.[1] Assuming that this value is approximately the same for a 1/4-inch-diameter wire, the bond stress may be calculated as

$$u_m = \frac{2 f_s A_s}{L' (\Sigma o)} = \frac{2\,(102,400)\,(0.05)}{20\,(0.786)} = 650 \text{ psi}$$

$$u_{avg} = \frac{1}{2} u_m = 325 \text{ psi}$$

The average bond failure (160 to 220 psi) generally occurs when the flexural cracks spread out from mid-span to the ends.

It is thus concluded that the beam failed in bond when the flexural cracks developed at 23.6 inches from the support (theoretically), which caused an increase in steel stress there.

Appendix E

STATIC LOAD-DEFLECTION CURVES AND STATIC LOAD-STRAIN CURVES FOR BEAMS B, H, AND K

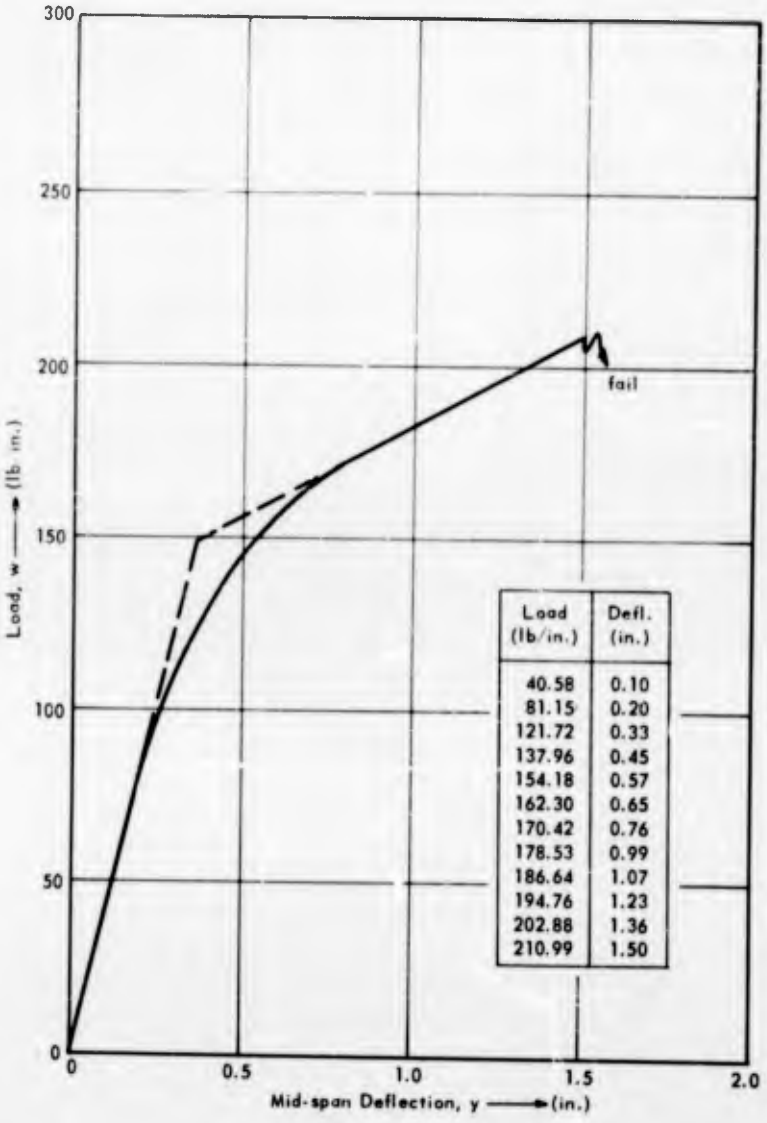

Figure E-1. Static load-deflection curve for Beam B.

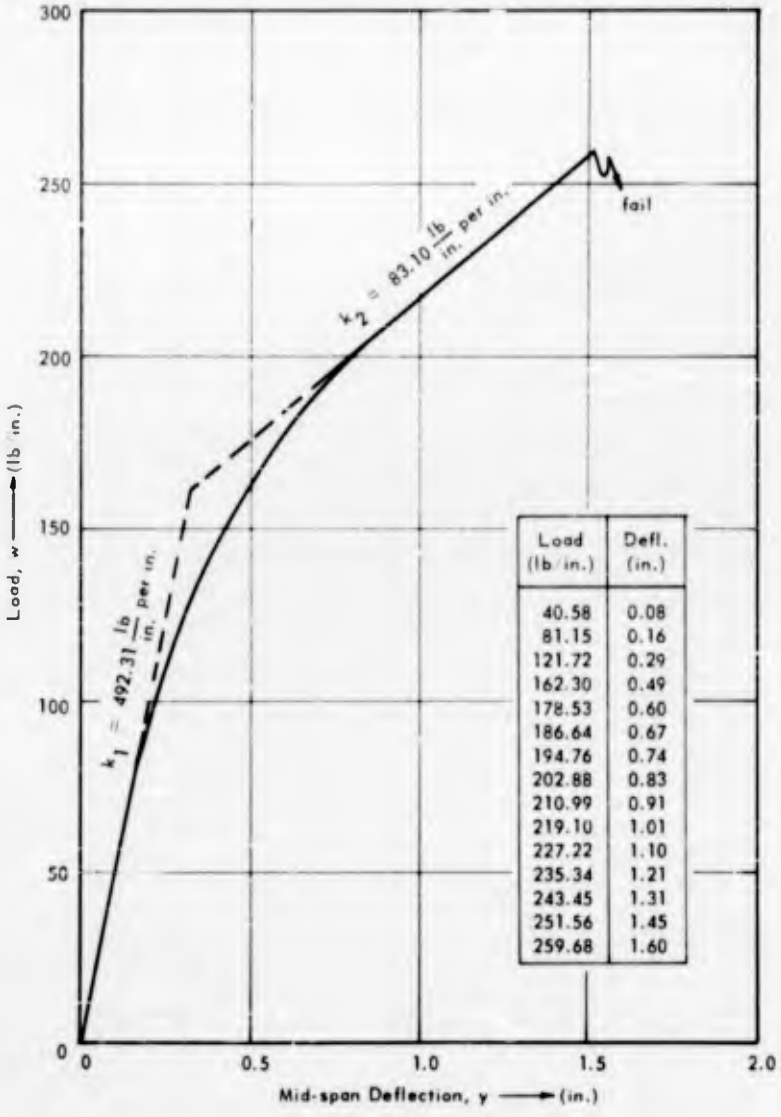

Figure E-2. Static load-deflection curve for Beam H.

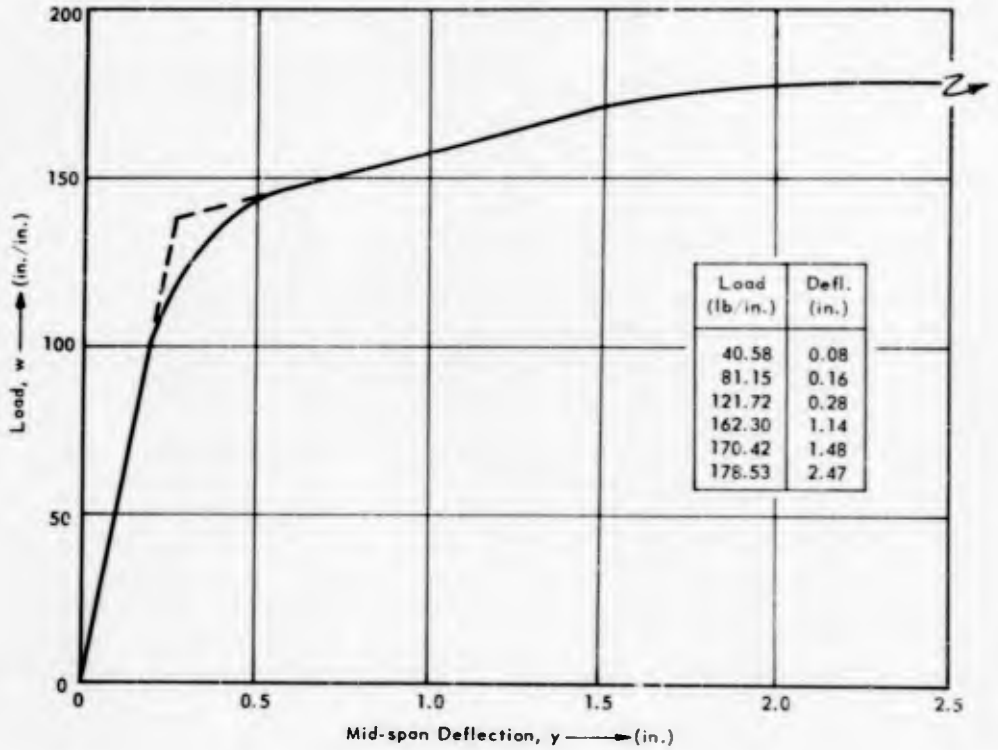

Figure E-3. Static load-deflection curve for Beam K.

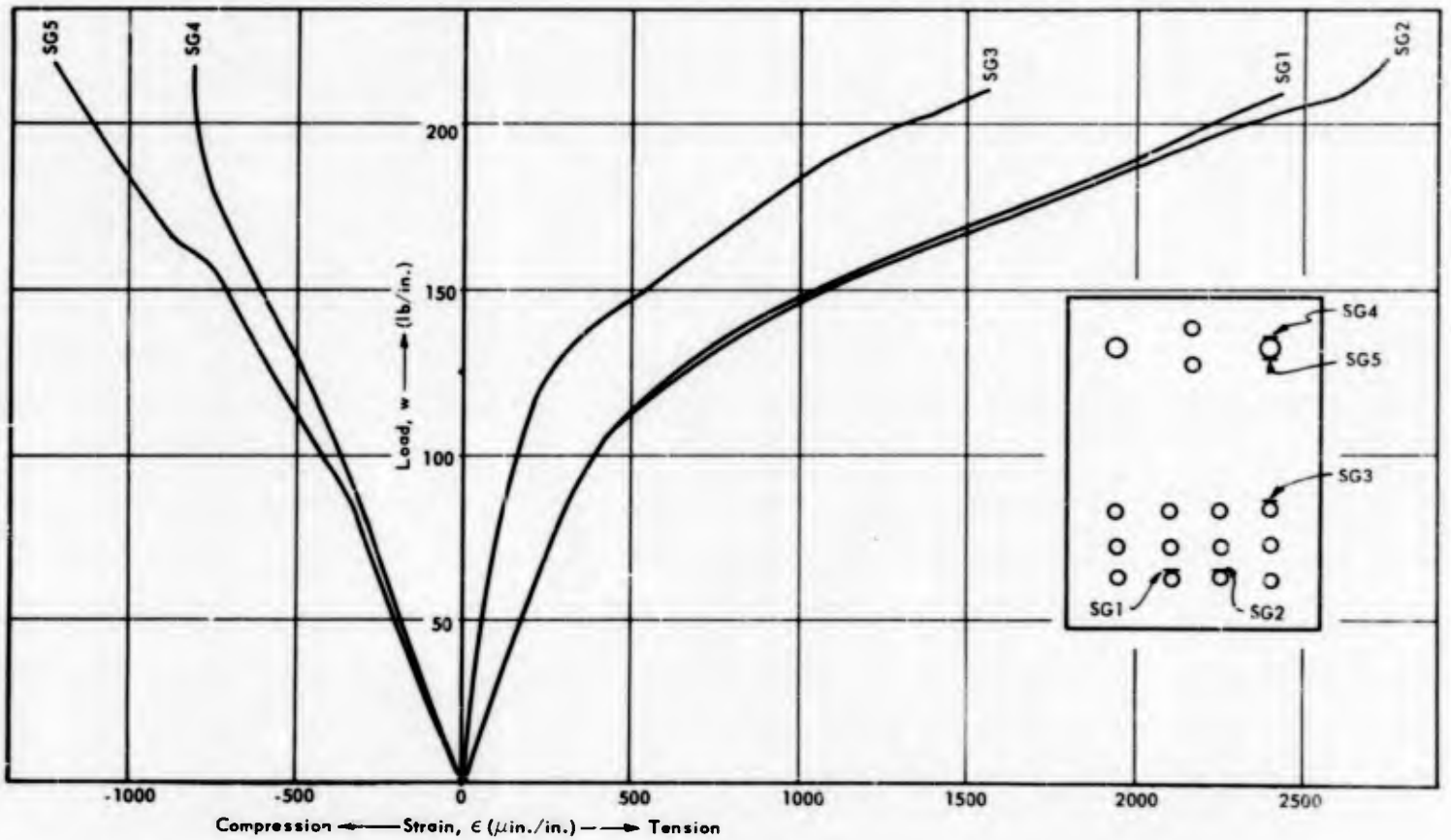

Figure E-4. Static load-strain curve for Beam B.

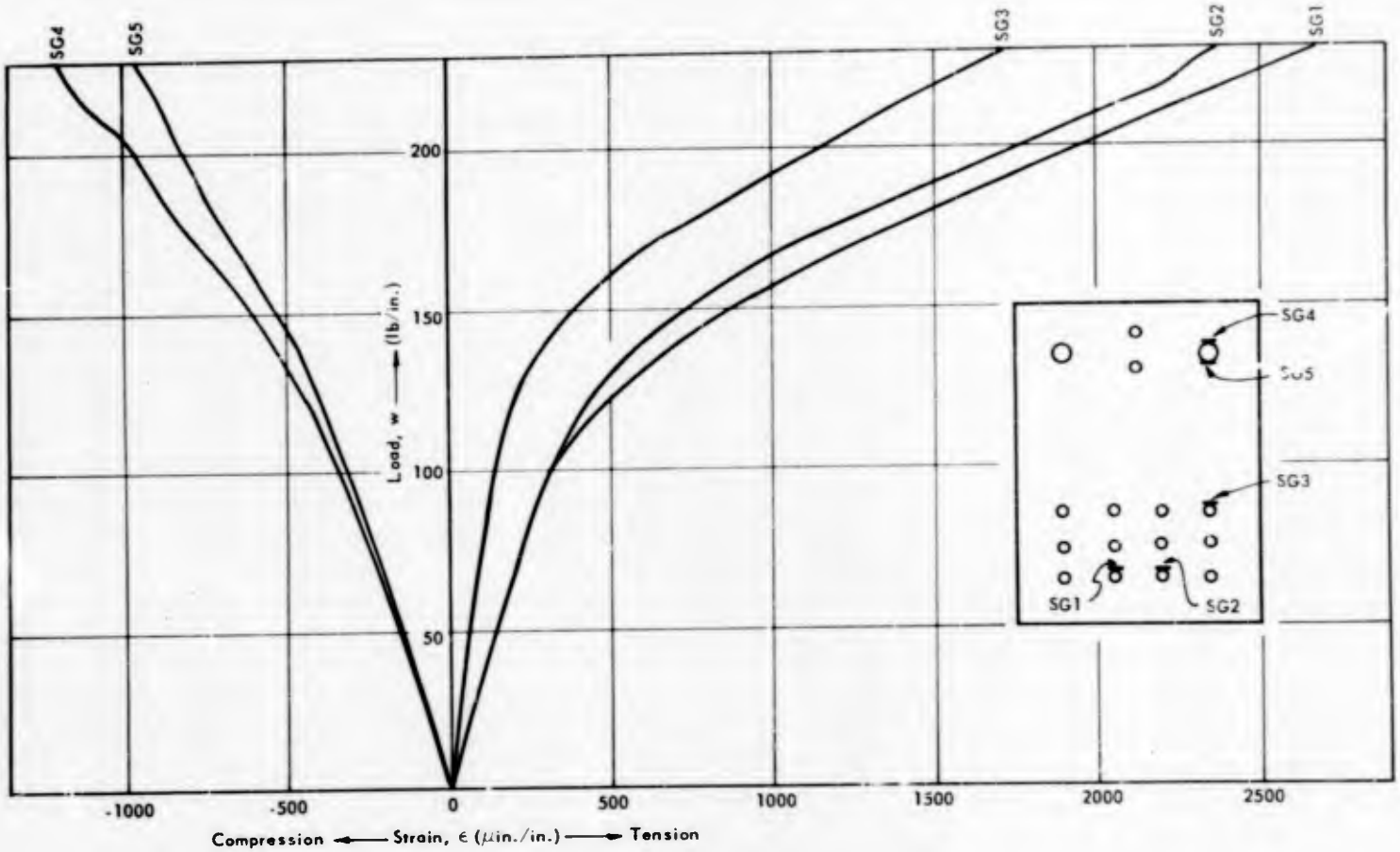

Figure E-5. Static load-strain curve for Beam H.

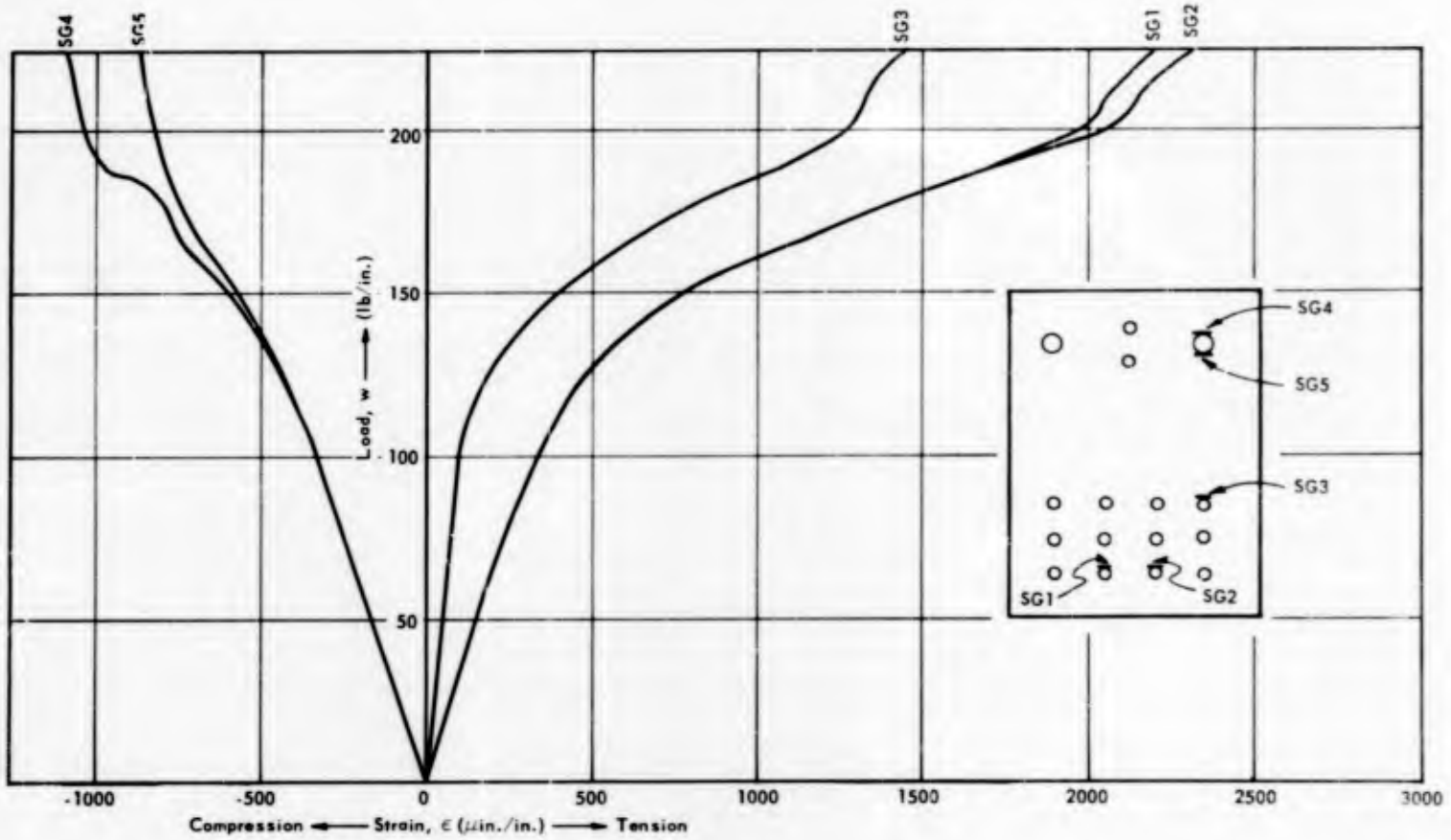

Figure E-6. Static load-strain curve for Beam K.

Appendix F

DEFLECTION-TIME CURVES RECORDED BY ROTATING DRUM

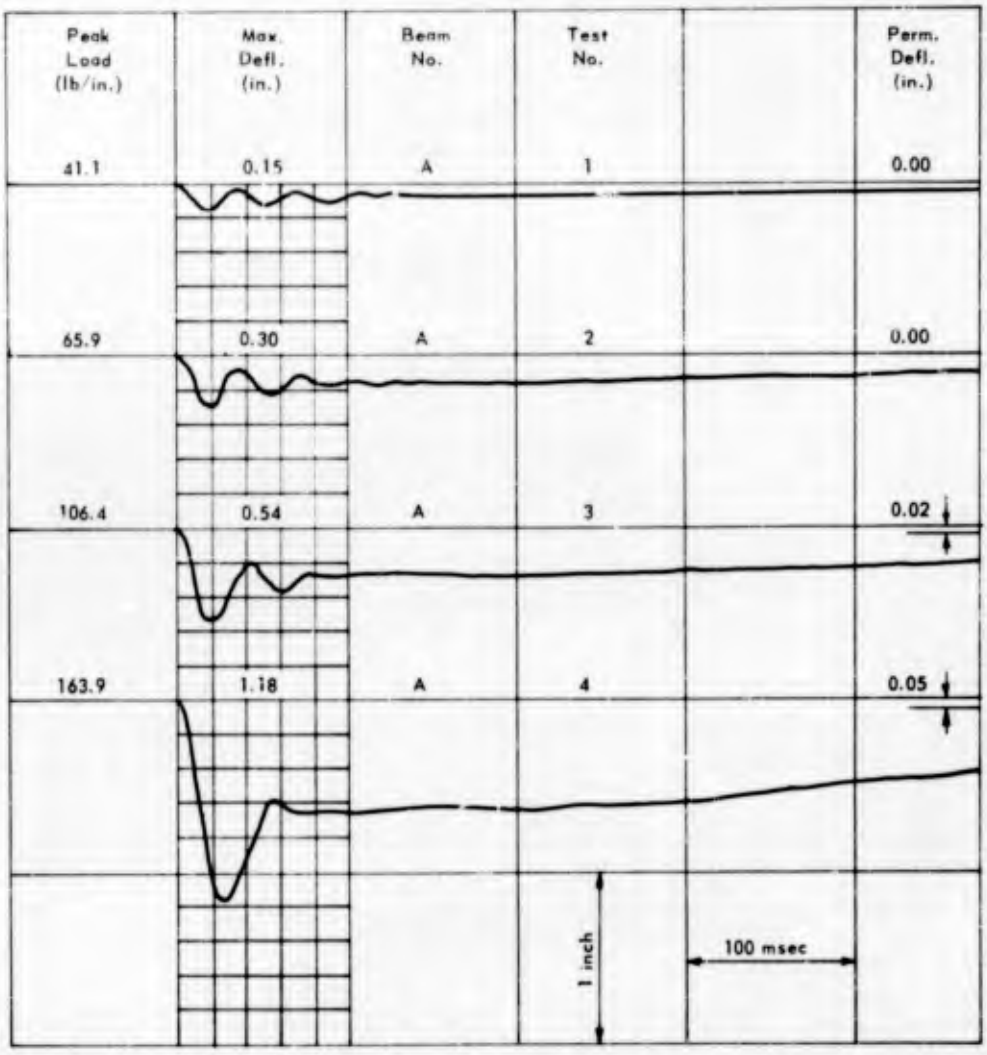

Figure F-1. Deflection-time curves, Beam A.

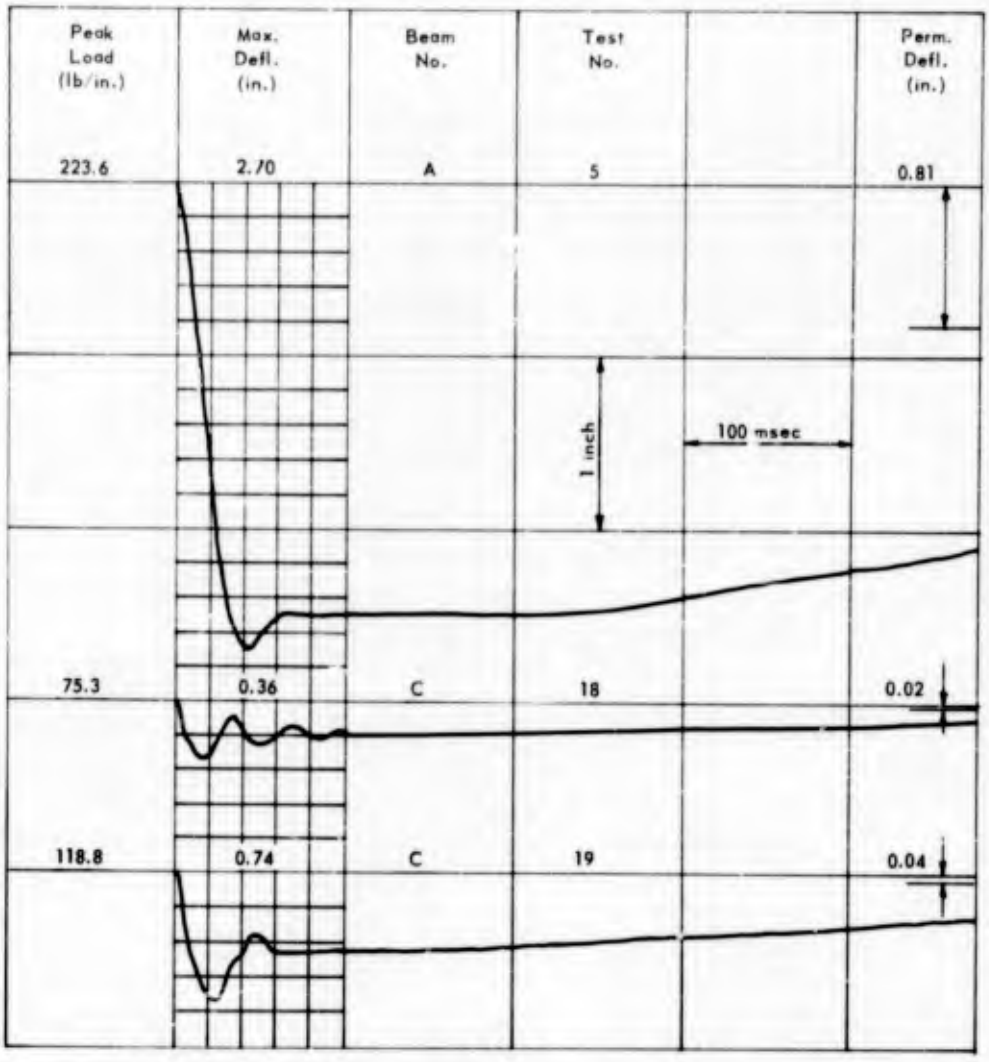

Figure F-2. Deflection-time curves, Beams A and C.

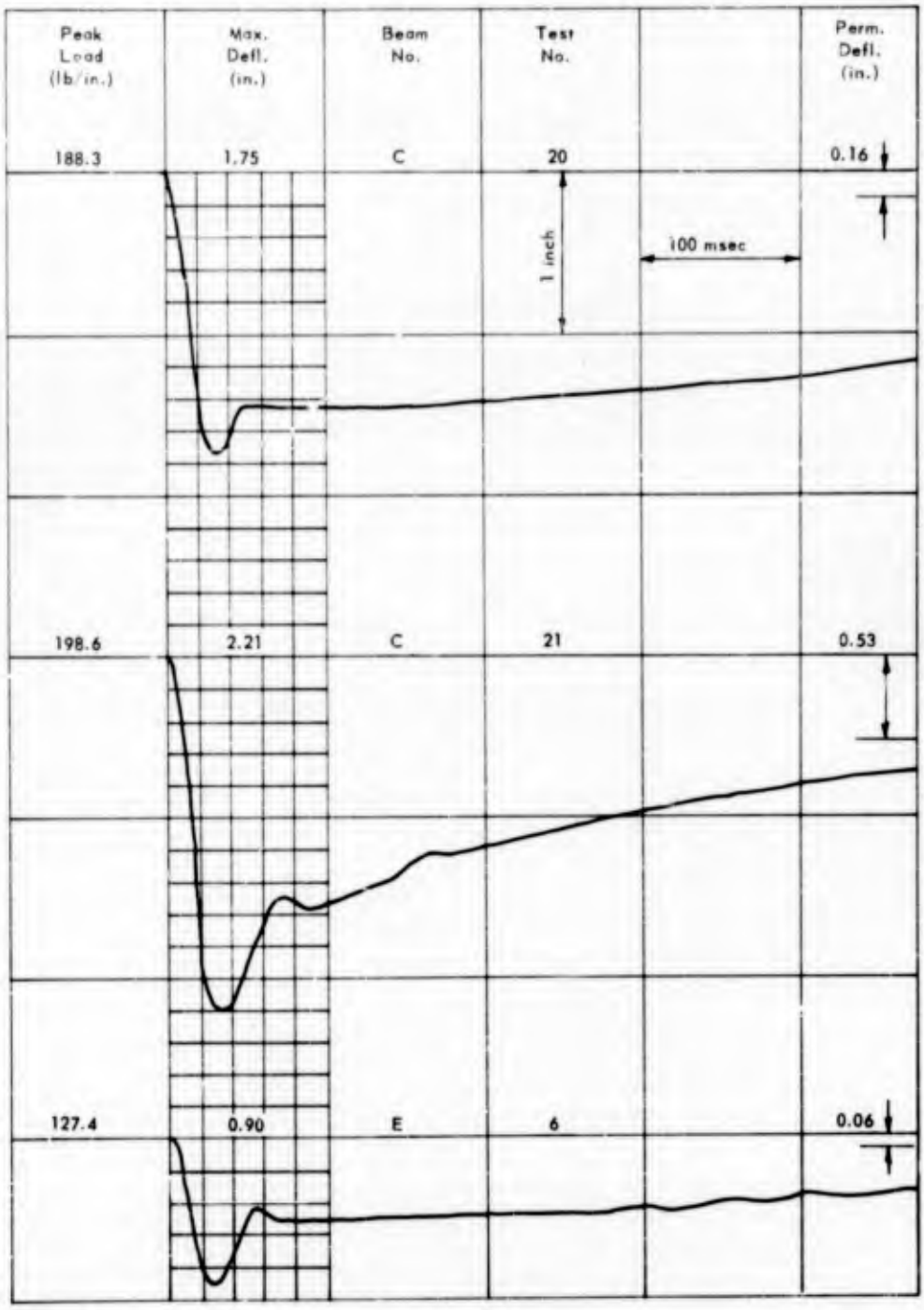

Figure F-3. Deflection-time curves, Beams C and E.

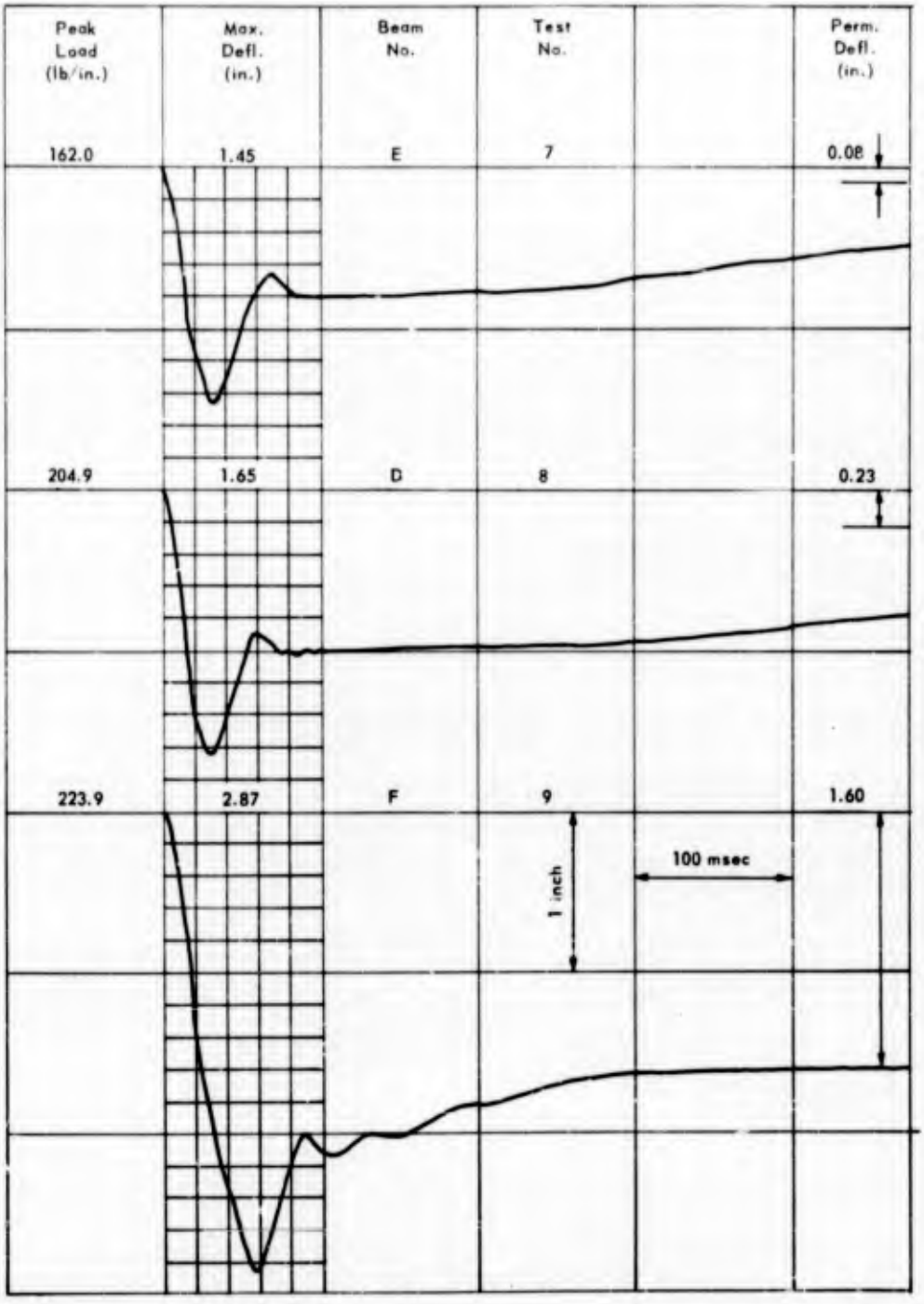

Figure F-4. Deflection-time curves, Beams D, E and F.

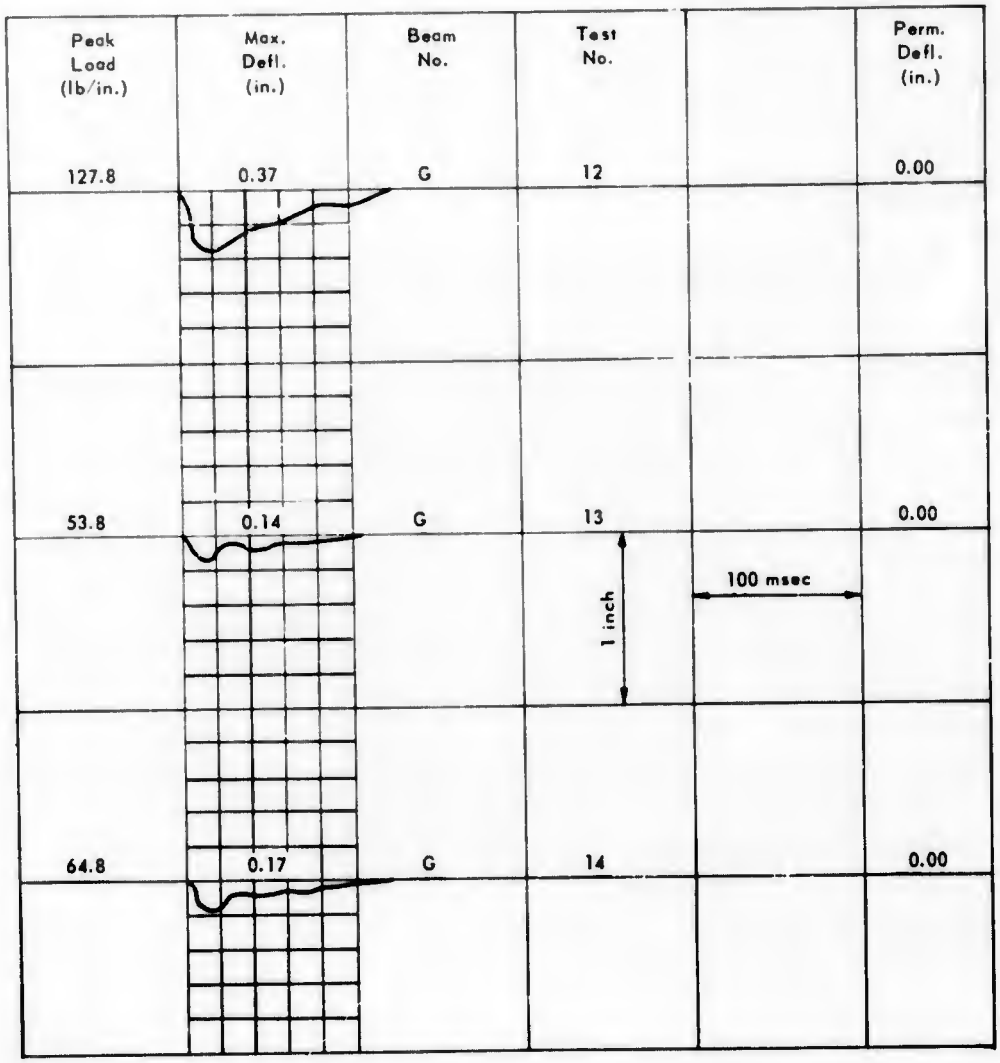

Figure F-5. Deflection-time curves, Beam G.

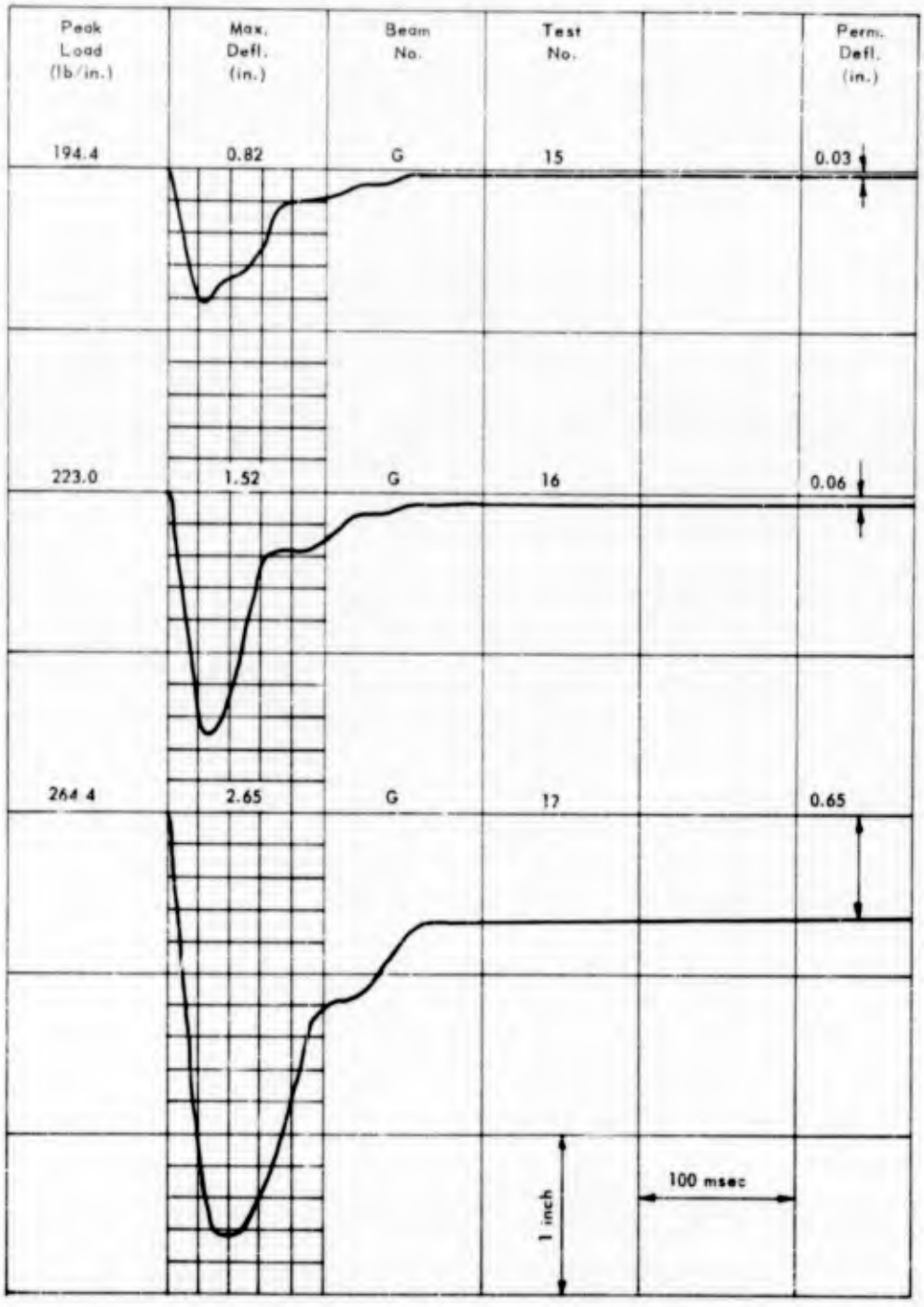

Figure F-6. Deflection-time curves, Beam G.

DISTRIBUTION LIST

No. of copies	SNDL Code	
25		Chief, Defense Atomic Support Agency, Washington, D. C.
10		Chief, Bureau of Yards and Docks (Code 70)
1	23A	Naval Forces Commanders (Taiwan Only)
4	39B	Construction Battalions
10	39D	Mobile Construction Battalions
3	39E	Amphibious Construction Battalions
2	39F	Construction Battalion Base Units
1	A2A	Chief of Naval Research - Only
2	A3	Chief of Naval Operation (OP-07, OP-04)
5	A5	Bureaus
2	B3	Colleges
2	E4	Laboratory ONR (Washington, D. C. only)
1	E5	Research Office ONR (Pasadena only)
1	E16	Training Device Center
7	F9	Station - CNO (Boston; Key West; San Juan; Long Beach; San Diego; Treasure Island; and Rodman, C. Z. only)
5	F17	Communication Station (San Juan; San Francisco; Pearl Harbor; Adak, Alaska; and Guam only)
1	F21	Administration Command and Unit CNO (Saipan only)
1	F40	Communication Facility (Pt. Lyautey only)
1	F41	Security Station
2	F42	Radio Station (Oso and Cheltenham only)
1	F48	Security Group Activities (Winter Harbor only)
8	H3	Hospital (Chelsea; St. Albans, Portsmouth, Va; Beaufort; Great Lakes; San Diego; Oakland; and Camp Pendleton only)
1	H6	Medical Center
2	J1	Administration Command and Unit - BuPers (Great Lakes and San Diego only)
1	J3	U. S. Fleet Anti-Air Warfare Training Center (Virginia Beach only)
2	J4	Amphibious Bases
1	J19	Receiving Station (Brooklyn only)
1	J34	Station - BuPers (Washington, D. C. only)
1	J37	Training Center (Bainbridge only)
1	J46	Personnel Center
1	J48	Construction Training Unit
1	J60	School Academy
1	J65	School CEC Officers
1	J84	School Postgraduate
1	J90	School Supply Corps

Distribution List (Cont'd)

No. of copies	SNDL Code	
1	J95	School War College
1	J99	Communication Training Center
11	L1	Shipyards
4	L7	Laboratory - BuShips (New London; Panama City; Carderock; and Annapolis only)
5	L26	Naval Facilities - BuShips (Antigua; Turks Island; Barbados; San Salvador; and Eleuthera only)
1	L30	Submarine Base (Groton, Conn. only)
2	L32	Naval Support Activities (London & Naples only)
2	L42	Fleet Activities - BuShips
4	M27	Supply Center
7	M28	Supply Depot (Except Guantanamo Bay; Subic Bay; and Yokosuka)
2	M61	Aviation Supply Office
15	N1	BuDocks Director, Overseas Division
28	N2	Public Works Offices
7	N5	Construction Battalion Center
4	N6	Construction Officer-in-Charge
1	N7	Construction Resident-Officer-in-Charge
12	N9	Public Works Center
1	N14	Housing Activity
2	R9	Recruit Depots
2	R10	Supply Installations (Albany and Barstow only)
1	R20	Marine Corps Schools, Quantico
3	R64	Marine Corps Base
1	R66	Marine Corps Camp Detachment (Tengan only)
7	W1A1	Air Station
32	W1A2	Air Station
9	W1B	Air Station Auxiliary
4	W1C	Air Facility (Phoenix; Monterey; Oppama; Naha; and Naples only)
4	W1E	Marine Corps Air Station (Except Quantico)
1	W1F	Marine Corps Auxiliary Air Station
8	W1H	Station - BuWeps (Except Rota)
1		Deputy Chief of Staff, Research and Development, Headquarters, U. S. Marine Corps, Washington, D. C.
1		President, Marine Corps Equipment Board, Marine Corps School, Quantico, Va.
2		Library of Congress, Washington, D. C.

Distribution List (Cont'd)

No. of copies	
1	Chief of Staff, U. S. Army, Chief of Research and Development, Department of the Army, Washington, D. C.
1	Office of the Chief of Engineers, Assistant Chief of Engineering for Civil Works, Department of the Army, Washington, D. C.
1	Chief of Engineers, Department of the Army, Attn: Engineering R & D Division, Washington, D. C.
1	Chief of Engineers, Department of the Army, Attn: ENGCW-OE, Washington, D. C.
1	Director, U. S. Army Engineer Research and Development Laboratories, Attn: Information Resources Branch, Fort Belvoir, Va.
1	Headquarters, Wright Air Development Division, (WWAD-Library), Wright-Patterson Air Force Base, Ohio
3	Headquarters, U. S. Air Force, Directorate of Civil Engineering, Attn: AFOCE-ES, Washington, D. C.
2	Commander, Headquarters, Air Force Systems Command, Andrews Air Force Base, Washington, D. C.
1	Deputy Chief of Staff, Development, Director of Research and Development, Department of the Air Force, Washington, D. C.
1	Director, National Bureau of Standards, Department of Commerce, Connecticut Avenue, Washington, D. C.
2	Office of the Director, U. S. Coast and Geodetic Survey, Washington, D. C.
10	Armed Services Technical Information Agency, Arlington Hall Station, Arlington, Va.
2	Director of Defense Research and Engineering, Department of Defense, Washington, D. C.
2	Director, Division of Plans and Policies, Headquarters, U. S. Marine Corps, Washington, D. C.
2	Director, Bureau of Reclamation, Washington, D. C.
2	Commanding Officer, U. S. Naval Construction Battalion Center, Attn: Technical Division, Code 141, Port Hueneme, Calif.
2	Commanding Officer, U. S. Naval Construction Battalion Center, Attn: Material Department, Code 142, Port Hueneme, Calif.
1	Commanding Officer, Yards and Docks Supply Office, U. S. Naval Construction Battalion Center, Port Hueneme, Calif.
1	Commanding Officer, U. S. Army Chemical Corps, Research & Development Command, Washington, D. C.
1	Hdq. U. S. Air Force, Director of Research & Development, DCS/D, Washington, D. C., Attn: Combat Components Division.
1	Commanding Officer, Chemical Warfare Laboratories, Army Chemical Center, Md.
1	U. S. Army Chemical Center, Nuclear Defense Laboratory, Edgewood, Md.
1	Prof. Allen F. Dill, Dept. of Civil Engineering, University of Illinois, Urbana, Ill.
1	Prof. J. T. Hanley, Dept. of Civil Engineering, University of Illinois, Urbana, Ill.
1	Asst. Prof. J. Silverman, Dept. of Chemical Engineering, University of Maryland, College Park, Md.
1	Portland Cement Association, 5420 Old Orchard Road, Skokie, Ill., (Attn: Research Librarian)

No. of copies	
1	Commandant, Industrial College of the Armed Forces, Washington, D. C.
1	Commandant, U. S. Armed Forces Staff College, U. S. Naval Base, Norfolk, Va.
1	Chief, Bureau of Ships, Attn: Chief of Research and Development Division, Navy Department, Washington, D. C.
1	Officer in Charge, U. S. Navy Unit, Rensselaer Polytechnic Institute, Troy, N. Y.
1	Commander, Pacific Missile Range, Attn: Technical Director, Point Mugu, Calif.
1	Commander, U. S. Naval Shipyard, Attn: Material Laboratory, Brooklyn
1	Office of Naval Research, Branch Office, Navy No. 100, Box 39, FPO, New York
1	Office of the Chief of Engineers, Department of the Army, Washington, D. C., Attn: ENGMC-ED
1	Officer in Charge, CECOS (ATTN:ADCE Course), Port Hueneme, Calif.
1	Commander, Air Force Special Weapons Center, Kirtland Air Force Base, Albuquerque, N. M.
1	Commander, Field Command, Defense Atomic Support Agency, Box 5100, Albuquerque, N. M.
1	Director, Civil Effects Test Group, Atomic Energy Commission, (ATTN: Mr. K. L. Corsbie), Washington, D. C.
1	Office of Civil and Defense Mobilization, Attn: Mr. Ben Taylor, Battle Creek, Mich.
1	U. S. Atomic Energy Commission, Technical Information Service, P.O. Box 62, Oak Ridge, Tenn.
1	Commanding Officer and Director, U. S. Naval Radiological Defense Laboratory, San Francisco
1	Commander, Air Force Ballistic Missile Division, Air Research and Development Command, P.O. Box 262, Inglewood, Calif.
1	Office of the Chief of Engineers, Department of the Army, T-7, Gravelly Point, Washington, D. C., ATTN: ENGNB
1	Commanding Officer, Engineer Research and Development Laboratories, Fort Belvoir, Va.
1	Chief of Engineers, Department of the Army, Washington, D. C.
1	Director, Waterways Experiment Station, Corps of Engineers, U. S. Army, Vicksburg, Miss.
1	Commander, U. S. Naval Ordnance Lab., White Oak, Silver Springs, Md., Attn: EA, EU, and E
1	Commander, U. S. Naval Ordnance Test Station, China Lake, Calif.
1	Commanding Officer and Director, U. S. Naval Civil Engineering Laboratory, Port Hueneme, Calif., Attn: Code L31
1	Director, U. S. Naval Research Lab., Washington, D. C.
1	Commanding Officer and Director, David W. Taylor Model Basin, Washington, D. C., Attn: Library
1	Hq. USAF (AFTAC), Washington, D. C.
1	Air Force Intelligence Center, Hq. USAF, (AFCIN-3K 2), Washington, D. C.
1	Director, Air University Library, Maxwell AFB, Ala.
1	Commandant, USAF Institute of Technology, Wright-Patterson AFB, Ohio, Attn: MCLI-ITRIDL
1	Commander, Western Development Division (ARDC), P.O. Box 262, Inglewood, Calif.
1	Director, Weapons Systems Evaluation Group, OSD, Room 1E880, the Pentagon, Washington, D. C.
1	Chief of Engineers, DA, Washington, D. C., Attn: ENGNB and ENGEB

Distribution List (Cont'd)

No. of copies	
1	Chief of Ordnance, DA, Washington, D. C. Attn: ORDTN
1	Director, Special Weapons Development, Headquarters CONARC, Fort Bliss, Tex. Attn: Chester I. Peterson
1	Commanding General, Aberdeen Proving Ground, Aberdeen, Md., Attn: Director, BRL
1	Commanding General, The Engineer Center, Fort Belvoir, Va., Attn: Asst. Commandant, Engineer School
1	Commanding Officer, Engineer Research & Development Laboratory, Fort Belvoir, Va., Attn: Chief, Tech. Support Branch
1	Chief of Naval Operations, DN, Washington, D. C., Attn: OP-75
1	Chief of Naval Operations, DN, Washington, D. C., Attn: OP-03EG
1	Director of Naval Intelligence, DN, Washington, D. C., Attn: OP-922v
1	Chief, Bureau of Naval Weapons, DN, Washington, D. C.
1	Chief, Bureau of Ships, DN, Washington, D. C., Attn: Code 372 and Code 423
1	Chief of Naval Research, DN, Washington, D. C., Attn: Code 811
1	Superintendent, U. S. Naval Postgraduate School, Monterey, Calif.
1	Commanding Officer, Nuclear Weapons Training Center, Atlantic, Naval Base, Norfolk, Va., Attn: Nuclear Warfare Department
1	Commanding Officer, Nuclear Weapons Training Center, Pacific, Naval Station, North Island, San Diego, Calif.
1	Commanding Officer, U. S. Naval Damage Control Training Center, Naval Base, Philadelphia, Penn., Attn: ABC Defense Course
1	Commandant, Army War College, Carlisle Barracks, Penn., Attn: Library
1	Commandant, National War College, Washington, D. C., Attn: Class Rec. Library
1	Los Alamos Scientific Laboratory, P.O. Box 1663, Los Alamos, N. M., Attn: Report Librarian
1	Deputy Chief of Staff, Research & Development Headquarters, U. S. Marine Corps, Washington, D. C.
1	Deputy CCMLO for Scientific Activities, Washington, D. C.
1	U. S. Army, Attn: Director of Research and Development Group, Washington, D. C.
1	U. S. Army Corps of Engineers, Office of the District Engineer, St. Paul District, 1217 U.S.P.O. and Customs House, St. Paul, Minn.
1	Air Force Cambridge Research Center, Hanscom Field, Bedford, Mass.
1	Commander, Air Research & Development Command, Attn: Library, Andrews Air Force Base, Washington, D. C.
1	Director of Research, Air Force Special Weapons Center, Kirtland Air Force Base, N. M.
1	Chief, Physical Research Branch, Research Division, U. S. Department of Commerce, Bureau of Public Roads, Washington, D. C.
1	Operation Civil, University of California, Richmond Field Station, Berkeley, Calif.
1	Library, Engineering Department, Stanford University, Stanford, Calif.
1	Director, Engineering Research Institute, University of Michigan, Ann Arbor, Mich.

No. of copies	
1	Library, Engineering Department, University of California, 405 Hilgard Avenue, Los Angeles
1	Library, Battelle Institute, Columbus, Ohio
1	Library, University of Southern California, University Park, Los Angeles
1	Director, The Technological Institution, Northwestern University, Evanston, Ill.
1	Library, Institute of Technology, University of Minnesota, Minneapolis, Minn.
1	Library, California Institute of Technology, Pasadena, Calif.
1	Mr. J. O'Sullivan, The Mitre Corporation, P.O. Box 208, Lexington, Mass.
1	Administrator, National Aeronautics & Space Administration, 1512 "H" Street N.W., Washington, D. C.
1	Langley Research Center, NASA, Langley Field, Hampton, Va., Attn: Mr. John Stack
1	Chief, Classified Technical Library, Technical Information Service, U. S. Atomic Energy Commission, Washington, D. C., Attn: Mrs. Jean O'Leary
1	Dr. Walker Bleakney, Forestal Research Center Library, Aeronautical Sciences Bldg., Princeton University, Princeton, N. J., Attn: Librarian
1	Manager, Albuquerque Operations Office, U. S. Atomic Energy Commission, P.O. Box 5400, Albuquerque, N. M.
1	Director, USAF Project RAND, Via: U. S. Air Force Liaison Office, The RAND Corporation, 1700 Main Street, Santa Monica, Calif.
1	Sandia Corporation, Sandia Base, Albuquerque, N. M., Attn: Classified Document Division, (For M. L. Merritt)
1	Library, Engineering Department, University of California, Berkeley, Calif.
1	Library, Southwest Research Institute, San Antonio, Tex.
1	Mr. E. E. Shalowitz, Protective Construction, GSA Building, 19th and F Street, N.W., Washington, D. C.
1	Lt. Col. Russell J. Hutchinson, 052921, Office of the Engineer, Camp Wolters, Mineral Wells, Tex.
1	CAPT. A. B. Chilton, CEC, USN, U. S. Naval Civil Engineering Laboratory, Port Hueneme, Calif.
1	CDR. C. A. Grubb, CEC, USN, Public Works Center, Navy No. 128, FPO, San Francisco
1	LT. L. K. Donovan, CEC, USN, U. S. Naval Nuclear Power Unit, U. S. Army Engineer Center, P.O. Box 96, Fort Belvoir, Va.
1	CAPT. W. M. McLellon, CEC, USN, Public Works Officer, Charleston Naval Shipyard, Charleston, S. C.
1	CAPT. L. N. Saunders, Jr., CEC, USN, Task Force 43, U. S. Atlantic Fleet, Bldg. Temporary, 6th and Independence Avenue, Washington, D. C.
1	CDR. J. F. Clarke, CEC, USN, Area Public Works Office, Chesapeake, U. S. Naval Weapons Plant, Washington, D. C.
1	LCDR. C. Curione, CEC, USN, Public Works Center, Navy No. 128, FPO, San Francisco
1	Mr. G. H. Albright, The Pennsylvania State University, College of Engineering and Architecture, University Park, Penn.
1	CAPT. J. H. Barker, Jr., CEC, USN, U. S. Naval Missile Center, Point Mugu, Calif.
1	CDR. W. J. Christensen, CEC, USN, Bureau of Yards and Docks, Code 70, Washington, D. C.
1	CAPT. J. H. Lofland, Jr., CEC, USN, U. S. Naval Air Station, North Island, San Diego, Calif.

Distribution List (Cont'd)

No. of copies	
1	CAPT. W. A. McManus, CEC, USN, U. S. Naval Air Station, Norfolk, Va.
1	CDR. J. D. Andrews, CEC, USN, Supreme HDQTRS, Allied Powers in Europe, APO 55, New York
1	CDR. D. P. Cunning, CEC, USN, District Public Works Office, 4th Naval District, Naval Base, Philadelphia, Penn.
1	LCDR. W. J. Francy, CEC, USN, Southeast Division, Bureau of Yards and Docks, U. S. Naval Base, Charleston, S. C.
1	LCDR. H. A. Locke, CEC, USN, Camp Smedley D. Butler, U. S. Marine Corps, Navy No. 161, FPO, San Francisco
1	CDR. H. L. Murphy, CEC, USNR, District Public Works Office, 12th Naval District, San Bruno, Calif.
1	LCDR. W. H. Sturman, CEC, USN, U. S. Naval Mobile Construction Battalion 9, FPO, San Francisco
1	CDR. W. A. Walls, CEC, USN, Headquarters, Defense Atomic Support Agency, Washington, D. C.
1	CDR. E. M. Saunders, CEC, USN, Bureau of Yards and Docks, Code 74, Washington, D. C.
1	CDR. C. F. Krickenberger, CEC, USN, Bureau of Yards and Docks, Washington, D. C.
1	LCDR. B. S. Merrill, CEC, USN, U. S. Naval Station, Navy No. 138, FPO, New York
1	CDR. H. W. Stephens, CEC, USN, Atomic Energy Commission, Military Applications Div., Germantown, Md.
1	LCDR. R. C. Vance, CEC, USN, U. S. Naval School, CEC Officers, Port Hueneme, Calif.
1	LCDR. C. R. Whipple, CEC, USN Bureau of Yards and Docks, Washington, D. C.
1	LCDR. W. D. Wilson, CEC, USN, U. S. Naval Air Station, Jacksonville, Fla.
1	LCDR. N. W. Clements, CEC, USN, U. S. Naval Nuclear Power Unit, U. S. Army Engineer Center, P.O. Box 96, Fort Belvoir, Va.
1	LCDR. J. C. LeDoux, CEC, USN, U. S. Naval School, CEC Officers, Port Hueneme, Calif.
1	LT. I. D. Crowley, CEC, USN, U. S. Naval Civil Engineering Laboratory, Port Hueneme, Calif.
1	LT. R. B. Reeves, CEC, USN, Field Command, Defense Atomic Support Agency, Sandia Base, Albuquerque, N. M.
1	CAPT. Robert Crawford, USAF, Field Command, Defense Atomic Support Agency, Sandia Base, Albuquerque, N. M.
1	Dr. Robert J. Hansen, Massachusetts Institute of Technology, Cambridge, Mass.
1	Dr. Bruce G. Johnston, Department of Civil Engineering, The University of Michigan, Ann Arbor, Mich.
1	Mr. M. L. Whitfield, Southwest Research Institute, 8500 Culebra Road, San Antonio, Tex.
1	Dr. Carl Eckberg, Civil Engineering Department, Iowa State University, Ames, Iowa
1	Dr. Lewis V. Spencer, Chairman, Ottawa University, Ottawa, Kan.
1	Mrs. Shea L. Valley, CRTZS, Cambridge Research Center, Bedford, Mass.
1	CAPT. William D. Sheehan, U.S.A., Defense Atomic Support Agency, Washington, D. C.
1	Dr. David Kleinecke, University of California, Engineering Field Station, 1301 South 46th Street, Richmond, Calif.
1	Mr. L. Neal FitzSimons, Office of Civil Defense, OASD-OCD, Dept. of Defense, Pentagon - 3B285, Washington, D.
1	Dr. William Kreger, U. S. Naval Radiological Defense Laboratory, San Francisco
1	Mr. Richard Park, National Academy of Sciences, 2101 Constitution Avenue, Washington, D. C.

Distribution List (Cont'd)

No. of copies	
1	Mr. W. R. Perret, 5112, Sandia Corporation, Sandia Base, Albuquerque, N. M.
1	Dr. N. M. Newmark, Civil Engineering Hall, University of Illinois, Urbana, Ill.
1	Mr. Fred Sauer, Physics Department, Stanford Research Institute, Menlo Park, Calif.
1	Dr. Harold Brode, Rand Corporation, 1700 Main Street, Santa Monica, Calif.
1	Mr. William J. Taylor, Terminal Ballistics Laboratory, Aberdeen Proving Ground, Aberdeen Proving Ground, Md.
1	Dr. T. H. Schiffman, Armour Research Foundation of Illinois Institute of Technology, Technology Center, Chicago, Ill.
1	Dr. F. T. Mavis, Dean, College of Engineering, Glen L. Martin Institute of Technology, University of Maryland, College Park, Md.
1	Dr. Robert V. Whitman, Massachusetts Institute of Technology, Cambridge, Mass.
1	Mr. Kenneth Kaplan, Broadview Research Corporation, 1811 Trousdale Drive, Burlingame, Calif.
1	Professor J. Neils Thompson, Civil Engineering Department, University of Texas, Austin, Tex.
1	Mr. G. L. Arbuthnot, Waterways Experiment Station, P.O. Box 631, Vicksburg, Miss.
1	Professor E. H. Gaylord, Department of Civil Engineering, University of Illinois, Urbana, Ill.
1	Dr. W. J. Hall, Department of Civil Engineering, University of Illinois, Urbana, Ill.
1	Dr. J. D. Haltiwanger, Department of Civil Engineering, University of Illinois, Urbana, Ill.
1	Mr. J. T. Hanley, Department of Civil Engineering, University of Illinois, Urbana, Ill.
1	Professor W. H. Munse, Department of Civil Engineering, University of Illinois, Urbana, Ill.
1	Dr. Lynn Beedle, Department of Civil Engineering, Lehigh University, Bethlehem, Penn.
1	Dr. Edward O. Pfrang, Department of Civil Engineering, University of Delaware, Newark, Del.
1	Dr. W. J. Austin, Department of Civil Engineering, Rice University, Houston, Tex.
1	Dr. J. G. Hammer, The Rand Corporation, Santa Monica, Calif.
1	Dr. Ray E. Untrauer, Department of Civil Engineering, Iowa State University, Ames, Iowa
1	Dr. Peter Hoadley, Department of Civil Engineering, Vanderbilt University, Nashville, Tenn.
1	Dr. Wallace Prescott, Department of Civil Engineering, Tennessee Polytechnic Institute, Cookeville, Tenn.
1	Dr. Eric T. Clarke, Technical Operations, Inc., Burlingame, Mass.
1	Dr. E. E. Massey, Defense Research Board, Dept. of National Defense, Ottawa, Canada
1	Mr. Richard Park, Secretary, National Academy of Sciences, 2101 Constitution Ave., N.W., Washington, D. C.
1	Dr. Hans Tiller, Nuclear Defense Lab., Army Chemical Center, Md.
1	Major Fort Verser, DASA Dept. of Defense, Washington, D. C.
1	Mr. John Auxier, Oak Ridge National Lab., Oak Ridge, Tenn.
1	Dr. James O. Buchanan, Office of Emergency Planning, Winder Bldg., Room 512, Washington, D. C.
1	Mr. Charles M. Eisenhauer, Radiation Physics Laboratory, High Voltage Lab., National Bureau of Standards, Washington, D. C.
1	Mr. Jack C. Greene, Chief, Review and Evaluation Branch, Division of Research, Policy and Review, Office of Emergency Planning, Winder Bldg., Room 526, Washington, D. C.

occurred in the top fiber, and, for loads less than 85 percent of the ultimate, a permanent deformation is negligible.

A method of predicting static ultimate deflection, and a solution for dynamic response, including damping, are presented.

U. S. Naval Civil Engineering Laboratory.
Technical Report R-192.
STATIC AND DYNAMIC LOADING OF PRETENSIONED CONCRETE BEAMS, by S. K. Takahashi.
87 p. illus. 15 June 62. UNCLASSIFIED

Nine simply supported pretensioned beams were tested statically or dynamically in the blast simulator. In the dynamic tests, no tensile stresses occurred in the top fiber, and, for loads less than 85 percent of the ultimate, a permanent deformation is negligible.

A method of predicting static ultimate deflection, and a solution for dynamic response, including damping, are presented.

1. Pretensioned Concrete Beams — Static and Dynamic Loading
I. Takahashi, S. K.
II. Y-F008-10-102A

U. S. Naval Civil Engineering Laboratory.
Technical Report R-192.
STATIC AND DYNAMIC LOADING OF PRETENSIONED CONCRETE BEAMS, by S. K. Takahashi.
87 p. illus. 15 June 62. UNCLASSIFIED

Nine simply supported pretensioned beams were tested statically or dynamically in the blast simulator. In the dynamic tests, no tensile stresses occurred in the top fiber, and, for loads less than 85 percent of the ultimate, a permanent deformation is negligible.

A method of predicting static ultimate deflection, and a solution for dynamic response, including damping, are presented.

1. Pretensioned Concrete Beams — Static and Dynamic Loading
I. Takahashi, S. K.
II. Y-F008-10-102A

U. S. Naval Civil Engineering Laboratory.
Technical Report R-192.
STATIC AND DYNAMIC LOADING OF PRETENSIONED CONCRETE BEAMS, by S. K. Takahashi.
87 p. illus. 15 June 62. UNCLASSIFIED

Nine simply supported pretensioned beams were tested statically or dynamically in the blast simulator. In the dynamic tests, no tensile stresses occurred in the top fiber, and, for loads less than 85 percent of the ultimate, a permanent deformation is negligible.

A method of predicting static ultimate deflection, and a solution for dynamic response, including damping, are presented.

1. Pretensioned Concrete Beams — Static and Dynamic Loading
I. Takahashi, S. K.
II. Y-F008-10-102A

U. S. Naval Civil Engineering Laboratory.
Technical Report R-192.
STATIC AND DYNAMIC LOADING OF PRETENSIONED CONCRETE BEAMS, by S. K. Takahashi.
87 p. illus. 15 June 62. UNCLASSIFIED

Nine simply supported pretensioned beams were tested statically or dynamically in the blast simulator. In the dynamic tests, no tensile stresses occurred in the top fiber, and, for loads less than 85 percent of the ultimate, a permanent deformation is negligible.

A method of predicting static ultimate deflection, and a solution for dynamic response, including damping, are presented.

1. Pretensioned Concrete Beams — Static and Dynamic Loading
I. Takahashi, S. K.
II. Y-F008-10-102A

UNCLASSIFIED

UNCLASSIFIED